Aircraft Concept Development Using the Global Sensitivity Approach and Algebraic Technology Models

by

Brett Malone and William H. Mason

VPI-Aero-184

December 10, 1991

Supported by :

National Aeronautics and Space Administration
Langley Research Center
Grant No: NAG-1-224

and

The National Science Foundation
Grant DDM-9008451

Department of Aerospace And Ocean Engineering
Virginia Polytechnic Institute and State University
Blacksburg, VA 24061

Aircraft Concept Development Using the Global Sensitivity Approach and Algebraic Technology Models

by

Brett Malone and William H. Mason
Virginia Polytechnic Institute and State University

SUMMARY

An approach to the conceptual development of aircraft configurations using multidisciplinary optimization is presented. We combine the Global Sensitivity Equation method, parametric optimization, and algebraic representations of the various technologies to obtain a PC level methodology. The result is a powerful yet simple procedure for identifying key design issues. It can be used both to investigate technology integration issues very early in the design cycle, and to establish the information flow framework between disciplines for use in multidisciplinary optimization projects using more computationally intense representations of each technology. To illustrate the approach, an examination of the optimization of a short takeoff heavy transport aircraft is presented for numerous combinations of performance and technology constraints. We demonstrated new insight into the effect of the figure of merit (objective function) on aircraft configuration size and shape by examining combinations of several objective functions in the optimization procedure.

ACKNOWLEDGEMENTS

Support for this work was provided by Dr. J. Sobieski at the NASA Langley Research Center under grant NAG-1-224, "Pilot Project: Multidisciplinary Design Approach to Aircraft Design Education," and by the National Science Foundation under grant DDM-9008451, "Variable Complexity Design Strategies for Integrated Multidisciplinary Design Optimization." This support is gratefully acknowledged.

TABLE OF CONTENTS

LIST OF FIGURES

LIST OF TABLES

LIST OF SYMBOLS

a	-	Average deceleration in landing analysis
AR	-	Aspect ratio
$\mathbf{B_k}$	-	Approximation to the Hessian of the Lagrangian function
$C_{D_{Boat}}$	-	Boattail drag coefficient
$C_{D_{Cruise}}$	-	Cruise drag coefficient
C_{D_f}	-	Skin friction drag coefficient
C_{D_O}	-	Zero lift drag
$C_{D_{Pylon}}$	-	Engine pylon drag coefficient
$C_{D_{Upsweep}}$	-	Aft fuselage upsweep drag coefficient
$C_{D_{Wave}}$	-	Transonic wave drag coefficient
$C_{f_{ac}}$	-	Total aircraft friction coefficient
C_{fclm}	-	Fuel used in climb to cruise altitude multiplier
C_{f_i}	-	Friction coefficient for i^{th} component
C_{fix}	-	Fixed component weight multiplier factor
C_{FORM}	-	Form factor coefficient
$C_{L_{Cruise}}$	-	Cruise lift coefficient
$C_{l_{Limit}}$	-	Section lift coefficient limit
$C_{L_{Limit}}$	-	Total lift coefficient limit
$C_{L_{TO}}$	-	Lift coefficient at takeoff
d_k	-	Solution to the quadratic subproblem at the k^{th} iteration
E	-	Oswald efficiency factor
$\mathbf{F}$	-	Function of disciplines representing entire system
$\mathbf{F_i}$	-	Implicit formulation of i^{th} discipline analysis
$\mathbf{f_i}$	-	Function representing the i^{th} discipline analysis

$f(x)$	-	Objective function
$\mathbf{G}$	-	Global sensitivity matrix
$g_i(x)$	-	i^{th} constraint function
h	-	Cruise altitude
h_l	-	Height of obstacle in landing analysis
K_s	-	Wing structural technology factor
L/D	-	Lift to drag ratio
M	-	Mach number
M_{Crit}	-	Critical Mach number
M_{DD}	-	Drag divergent Mach number
M_o	-	Maximum Mach number
N	-	Ultimate load factor
R	-	Range
S_{air}	-	Air distance in landing calculation
S_{csw}	-	Wing mounted control surface area
sfc	-	specific fuel consumption (lb/lb/hr)
S_{ldg}	-	Landing ground roll
S_{to}	-	Takeoff distance
S_{ref}	-	Reference area
S_w	-	Wing area
S_{wet_i}	-	Wetted area for i^{th} component
t/c	-	Wing thickness ratio
T_{req}	-	Thrust required in cruise segment
T/W_{eng}	-	Thrust to weight ratio for engine
u_k	-	Vector of Lagrange multipliers

V	-	Cruise velocity
V_a	-	Landing approach velocity
v_k	-	Approximation to optimal Lagrange multipliers
V_{rot}	-	Rotation velocity at takeoff
V_{Td}	-	Landing touch down velocity
W_{cargo}	-	Cargo weight
W_{eng}	-	Engine weight
W_{fclm}	-	Fuel weight used in climb segment
W_{fix}	-	Fixed weight
W_{fuel}	-	Fuel weight used in cruise segment
$W_{Initial}$	-	Initial cruise weight
W_{to}	-	Takeoff gross weight
W_{wing}	-	Wing weight
$\mathbf{X}$	-	Vector of design variables
$\mathbf{X_k}$	-	Design variable set for k^{th} optimization iteration
$\mathbf{X_o}$	-	Vector of design variables for baseline design
$\mathbf{Y_i}$	-	Vector of key parameters for the i^{th} discipline
$\mathbf{Y_{i_o}}$	-	Solution of the i^{th} discipline
α_k	-	Steplength parameter
γ	-	Average drag-to-weight ratio at landing
λ	-	Taper ratio
Λ	-	Wing quarter-chord sweep
κ_a	-	Technology factor for drag divergent Mach number
Δn	-	Pilot performance factor in landing analysis

1. INTRODUCTION

Aircraft conceptual design is becoming an increasingly complicated process. To achieve advances in performance, each technology, or discipline, must be much more highly integrated than in the past. In addition, designs of interest often depart radically from past experience. The designer is forced to confront many issues immediately, and the initial decisions made will essentially dictate the cost and schedule of the project. Under these conditions, the designer needs tools that provide good insight into the key technology integration issues at the earliest possible time. Rapid system evaluation with good insight into the important design parameters is the key to a successful initial design.

Aircraft designers are acutely aware of the importance of initial sizing and optimization. One well known current method for aircraft sizing is ACSYNT (Aircraft Synthesis), which was originally described by Vanderplaats[1], and is undergoing continual development[2]. Although large, complicated sizing routines are extremely valuable, it would be useful to provide the designer with a simpler, PC level, rapid means of focusing directly on the issues arising from the integration of different disciplines in the complete system.

The problem of understanding how to combine different disciplines to achieve optimum designs has been addressed by Sobieski and co-workers for several years. This work has as its long term goal the establishment of a rational means of coupling the most powerful computational methodology available for each discipline. An overview of the work has been given recently by Sobieski[3], and the key idea of a Global Sensitivity Equation method to define interactions between disciplines has been described in detail in Ref. 4. This technique can provide an important alternative to more traditional sizing programs even though it is intended to address more detailed design problems.

Applications of this methodology have been described in references 5,6, and 7. NASA experience is described in reference 8.

Analytic technology models have been demonstrated to provide an excellent means of understanding technology integration issues recently by Mason[9]. Using very simple algebraic models, the key interactions between structures, propulsion and aerodynamics were demonstrated. Considering the value of both simple and sophisticated analysis in design, it appears reasonable to combine both levels of simulation in a single design methodology. This has been done using a concept called "Variable Complexity Design" by Unger[10], et al. This concept can be applied in numerous ways to specific design problems. Another example is the "Combined Global-Local Approximation" approach proposed by Haftka[11].

This thesis describes an approach which combines aspects of the methods described above for use by designers during early stages of configuration feasibility studies. The purpose is to provide insight into the key design issues with minimum effort. Analytic technology models are defined, and the approach is structured so that they can be replaced by improved models as desired. Sobieski's Global Sensitivity Equation (GSE) method is then used to determine the interactions between disciplines. With the gradients of the design available from the GSE analysis, a solution to the numerical optimization problem can be obtained.

After a review of the mathematical basis of the GSE method, the technology models are defined. Using a short takeoff heavy transport as an example, the results from both the GSE analysis and the optimization are presented. Due to the simplicity of the approach, results of nearly a hundred optimizations are used to illustrate the effects of various design variables, design Mach number, range, takeoff distance, and different complexity analysis.

2. Review of a Global Sensitivity Equation Theory

As stated in the introduction, the methodology that leads to the sensitivities for a highly coupled, nonlinear system is given in detail by Sobieski in Ref. 4. This approach is known as the Global Sensitivity Equation Theory. The objective of this thesis is to use this methodology in conjunction with analytic models to illustrate the interdependence of various aircraft technologies. We describe the individual technologies, or disciplines, as the subsystems to the entire aircraft being designed. These subsystems include, for example, aerodynamics, structures, and propulsion. Within each subsystem are the individual parameters that are key to the design process. These include such items as takeoff field length, or wing weight. In the traditional design approach, these subsystems would be treated individually, allowing little or no communication with the other subsystems in the process of gradient computations in the optimization process. However, in order to obtain an optimum design, we must recognize that these disciplines are highly coupled, and that this coupling must be captured to calculate accurate and meaningful derivatives.

By coupling, we mean that the influence of one discipline's output, or key parameter, on another discipline's output is measured and used to augment that parameter's gradient with respect to a certain design variable. For instance, a gradient of takeoff gross weight with respect to a specific design variable would normally involve a finite difference calling only the weights subsystem. This type of sensitivity is known as a local derivative. When this approach is taken, however, the important influences of the aerodynamics subsystem are not considered. The solution for the takeoff gross weight is an iterative procedure that depends heavily on the relationship between these two disciplines. As a result, the coupling effects between the two disciplines must be

quantified. The solution to the Global Sensitivity Equations (GSE) provides this coupling. The GSE sensitivities capture the overall system response by using the local derivatives and the computed system coupling to solve for the global derivatives.

2.1 Formulation of the Global Sensitivity Equations

To illustrate the theory of the GSE method, we define a complex, coupled system as a process whose actions can be described by a solution vector $\mathbf{Y}$ that can be obtained from a set of simultaneous equations, partitioned into separate subsets. The problem of sizing an aircraft can be described as the solution to the set of simultaneous equations given by the various technologies. Thus, we begin considering these technologies as the subsets to the entire system, the aircraft. For example, if the disciplines chosen were aerodynamics, weights, and propulsion, the set of equations that describe the entire, coupled system can be written as follows.

$$\begin{aligned} \mathbf{Aero}\left[\left(\mathbf{X}, \mathbf{Y}_{Weights}, \mathbf{Y}_{Prop}\right), \mathbf{Y}_{Aero}\right] &= 0 \\ \mathbf{Weights}\left[\left(\mathbf{X}, \mathbf{Y}_{Aero}, \mathbf{Y}_{Prop}\right), \mathbf{Y}_{Weights}\right] &= 0 \\ \mathbf{Prop}\left[\left(\mathbf{X}, \mathbf{Y}_{Aero}, \mathbf{Y}_{Weights}\right), \mathbf{Y}_{Prop}\right] &= 0 \end{aligned} \tag{1}$$

where X is the set of design variables, an independent set that is used in each subset.

The disciplines described above represent separate analysis that can range in complexity from simple analytic representations to elaborate computational analysis. These disciplines yield solution vectors in the form of $\mathbf{Y}_i$, where i is the identifier for the subset that produces the solution.

We see from Eqn (1) that the disciplines are coupled because the input to one discipline includes the outputs of the other disciplines. An example of this relationship is

the need to know the aircraft weight in order to compute the cruise lift coefficient. The coupling of the entire system can be represented graphically as seen in Figure 1.

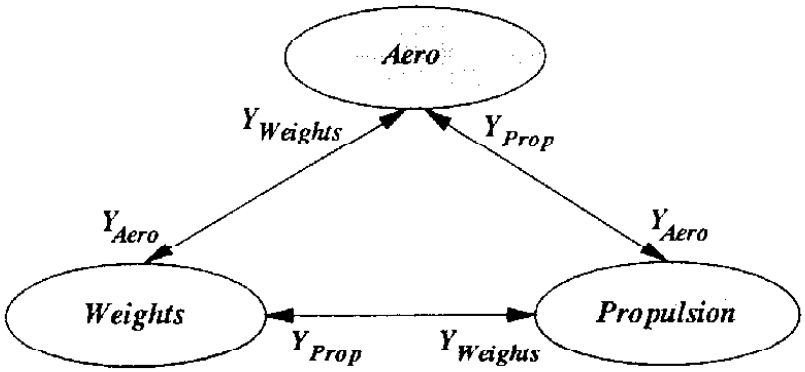

Figure 1. Coupling Representation of Disciplines.

The solution to the system is the solution to the coupled set of equations. This can be represented as the solution to the following,

$$\mathbf{F(Y,X) = 0} \tag{2}$$

If we consider that **Y** can be described as,

$$\mathbf{Y = f(X)} \tag{3}$$

then by the implicit function theorem[12], we can write the corresponding sensitivity equation to the above set as,

$$\left\{\frac{\mathbf{DF}}{\mathbf{DX}}\right\} = \left\{\frac{\partial \mathbf{F}}{\partial \mathbf{X}}\right\} + \left[\frac{\partial \mathbf{F}}{\partial \mathbf{Y}}\right]\left\{\frac{\partial \mathbf{Y}}{\partial \mathbf{X}}\right\} = 0 \tag{4}$$

or,

$$\left[\frac{\partial \mathbf{F}}{\partial \mathbf{Y}}\right]\left\{\frac{\partial \mathbf{Y}}{\partial \mathbf{X}}\right\} = -\left\{\frac{\partial \mathbf{F}}{\partial \mathbf{X}}\right\} \tag{5}$$

The partitions of the **Y** vector can be written in terms of the design variables, **X**, and the remaining partitions of **Y** to follow the form of Eqn (3).

$$\mathbf{Y}_{Aero} = \mathbf{f}_{Aero}(\mathbf{Y}_{Weights}, \mathbf{Y}_{Prop}, \mathbf{X}) \tag{6a}$$

$$\mathbf{Y}_{Weights} = \mathbf{f}_{Weights}(\mathbf{Y}_{Aero}, \mathbf{Y}_{Prop}, \mathbf{X}) \tag{6b}$$

$$\mathbf{Y}_{Prop} = \mathbf{f}_{Prop}(\mathbf{Y}_{Aero}, \mathbf{Y}_{Weights}, \mathbf{X}) \tag{6c}$$

We can now linearize the system of equations shown in Eqns (6) in the neighborhood of the solution, $\mathbf{Y}_{io}$, using a Taylor series expansion. Shown here is only the $\mathbf{Y}_{Aero}$ subset.

$$\mathbf{Y}_{Aero} = \mathbf{Y}_{Aero_o} + \frac{\partial \mathbf{f}_{Aero}}{\partial \mathbf{X}}\Delta\mathbf{X} + \frac{\partial \mathbf{f}_{Aero}}{\partial \mathbf{Y}_{Weights}}\Delta\mathbf{Y}_{Weights} + \frac{\partial \mathbf{f}_{Aero}}{\partial \mathbf{Y}_{Prop}}\Delta\mathbf{Y}_{Prop} \tag{7}$$

If we then rearrange the set of linearized equations to reflect the form of Eqn (1), we can write,

$$\mathbf{Aero} = \mathbf{Y}_{Aero} - \mathbf{Y}_{Aero_o} - \frac{\partial \mathbf{f}_{Aero}}{\partial \mathbf{X}}\Delta\mathbf{X} - \frac{\partial \mathbf{f}_{Aero}}{\partial \mathbf{Y}_{Weights}}\Delta\mathbf{Y}_{Weights} - \frac{\partial \mathbf{f}_{Aero}}{\partial \mathbf{Y}_{Prop}}\Delta\mathbf{Y}_{Prop} = \mathbf{0} \tag{8}$$

and, thus,

$$\mathbf{F} = \begin{Bmatrix} \mathbf{Aero} \\ \mathbf{Weights} \\ \mathbf{Prop} \end{Bmatrix} = 0 \tag{9}$$

We can now apply the implicit function theorem to the linearized set of equations (8) by differentiating as shown in Eqn (5). This leads to the global sensitivity equations, given by,

$$\begin{bmatrix} \mathbf{I} & -\frac{\partial \mathbf{f}_{Aero}}{\partial \mathbf{Y}_{Weights}} & -\frac{\partial \mathbf{f}_{Aero}}{\partial \mathbf{Y}_{Prop}} \\ -\frac{\partial \mathbf{f}_{Weights}}{\partial \mathbf{Y}_{Aero}} & \mathbf{I} & -\frac{\partial \mathbf{f}_{Weights}}{\partial \mathbf{Y}_{Prop}} \\ -\frac{\partial \mathbf{f}_{Prop}}{\partial \mathbf{Y}_{Aero}} & -\frac{\partial \mathbf{f}_{Prop}}{\partial \mathbf{Y}_{Weights}} & \mathbf{I} \end{bmatrix} \begin{Bmatrix} \frac{D\mathbf{Y}_{Aero}}{D\mathbf{X}} \\ \frac{D\mathbf{Y}_{Weights}}{D\mathbf{X}} \\ \frac{D\mathbf{Y}_{Prop}}{D\mathbf{X}} \end{Bmatrix} = \begin{Bmatrix} \frac{\partial \mathbf{f}_{Aero}}{\partial \mathbf{X}} \\ \frac{\partial \mathbf{f}_{Weights}}{\partial \mathbf{X}} \\ \frac{\partial \mathbf{f}_{Prop}}{\partial \mathbf{X}} \end{Bmatrix} \tag{10}$$

The right-hand-side of equation (10) is the sensitivity of each discipline with respect to the independent variable, or the design variable set. These are local derivatives. There is a different right-hand-side for each design variable. The solution of the system (10) is the sensitivity of the partitioned vector **Y** with respect to the design variable set **X**. These are the global derivatives. The derivatives of **Y** represent the system sensitivity with all of the effects of the discipline couplings accounted for.

There is a full set of these derivatives for every design variable, therefore, the system must be solved for each design variable. This can be efficiently done by decomposing the GSE matrix once, and then solving repeatedly for each right-hand-side. Once the global derivatives are found, this information can then be supplied to the optimization routine for search direction calculation.

We note that each component of the GSE matrix is a matrix within itself. If, for instance, we have a number of subsystem parameters within a certain discipline, then that one component within the GSE matrix would look like,

$$\frac{\partial \mathbf{f}_{Aero}}{\partial \mathbf{Y}_{Weights}} = \begin{bmatrix} \frac{\partial \mathbf{f}_{Aero}(1)}{\partial \mathbf{Y}_{Weights}(1)} & \cdots & \frac{\partial \mathbf{f}_{Aero}(1)}{\partial \mathbf{Y}_{Weights}(n_W)} \\ \vdots & \ddots & \vdots \\ \frac{\partial \mathbf{f}_{Aero}(n_A)}{\partial \mathbf{Y}_{Weights}(1)} & \cdots & \frac{\partial \mathbf{f}_{Aero}(n_A)}{\partial \mathbf{Y}_{Weights}(n_W)} \end{bmatrix} \tag{11}$$

2.2 Normalizing for the Optimization

For numerical accuracy in the use of optimization programs, it is important to supply gradients that are all of the same order. For instance, it is numerically inferior to supply a gradient of one design variable that is on the order of 10^4 and supply another gradient that is on the order of 10^{-4}. Instead, the gradients should be normalized by using the solution to the baseline system, given by $\mathbf{Y}_{Aero_o}$, $\mathbf{Y}_{Weights_o}$, and $\mathbf{Y}_{Prop_o}$.

The derivatives are then found, as described in the previous section, and normalized in the following manner.

Derivatives in the GSE matrix are normalized with respect to the discipline solutions,

$$\left.\frac{\partial \mathbf{f}_{Aero}(\mathrm{i})}{\partial \mathbf{Y}_{Weights}(\mathrm{j})}\right|_o = \frac{\partial \mathbf{f}_{Aero}(\mathrm{i})}{\partial \mathbf{Y}_{Weights}(\mathrm{j})} \cdot \frac{\mathbf{Y}_{Weights_o}(\mathrm{j})}{\mathbf{f}_{Aero_o}(\mathrm{i})} \tag{12}$$

and for the local gradient vector, with respect to the baseline design variables,

$$\left.\frac{\partial \mathbf{f}_{Aero}(\mathrm{i})}{\partial \mathbf{X}(\mathrm{j})}\right|_o = \frac{\partial \mathbf{f}_{Aero}(\mathrm{i})}{\partial \mathbf{X}(\mathrm{j})} \cdot \frac{\mathbf{X}_o(\mathrm{j})}{\mathbf{f}_{Aero_o}(\mathrm{i})} \tag{13}$$

3. TECHNOLOGY MODELS

In this analysis, the aircraft takeoff gross weight, W_{to}, will be the key figure of merit. W_{to} is defined to consist of:

$$W_{to} = W_{wing} + W_{fuel} + W_{eng} + W_{fixed} + W_{fclm} + W_{cargo} \tag{14}$$

The main purpose of this optimization procedure is to find the wing design, fuel required, and engine size required to minimize the total aircraft weight for the specified mission and field performance. Components other than the wing and fuel weight were taken to be either fractions of the takeoff weight, or prescribed constants. For initial development, ACSYNT[2] was used to obtain accurate weight fractions.

3.1 Weights

3.1.1 Structures

The wing structural weight can be estimated using wing weight equations. Several levels of approximations are available. The equation from Raymer[13] for subsonic transports is one example:

$$W_{wing} = 0.0051\, K_s S_w^{0.649} S_{csw}^{0.1} \frac{AR^{0.5}}{(t/c)_{root}^{0.4}} \cdot \frac{(N W_{to})^{0.557} (1+\lambda)^{0.1}}{\cos \Lambda_{.25}} \tag{15}$$

The weight prediction from this equation was checked against data in Torenbeek[14] for typical transports and found to be accurate to within 2-3%.

3.1.2 Fuel Weight

The weight of fuel used in the cruise segment of the mission is found using the Brequet range equation.

$$W_{Fuel} = W_{Initial}\left(1 - e^{\left\{-\frac{R \cdot sfc}{V(L/D)}\right\}}\right) \tag{16}$$

This formulation takes $W_{Initial}$ as the weight of the aircraft at the start of the cruise segment. $W_{Initial}$ is simply the takeoff weight less the weight of the fuel used to climb to the cruise altitude.

$$W_{Initial} = W_{to} - W_{fclm} \tag{17}$$

3.1.3 Engine Weight

The engine weight is found based on a required thrust and a specified thrust to weight ratio for the class of propulsion system selected. Thus the engine weight is found from,

$$W_{eng} = \frac{T_{req}}{(T/W)_{eng}} \tag{18}$$

Specific fuel consumption can be constant, or vary if information is available.

3.1.4 Systems / Miscellaneous

The remaining weights can be defined as aircraft structure and systems weight excluding the wing structural weight. This weight can be expressed as a fraction of the takeoff gross weight.

$$W_{fix} = C_{fix} W_{to} \tag{19}$$

Here, we define C_{fix} as the percentage of the takeoff weight that the system represents. The fixed weight here refers to remaining structural weight, furnishings, landing gear, etc. By defining the variables that do not change as a direct result of the changes in the design variables in this manner, these aircraft systems are sized automatically with the changes in the takeoff weight. This method is also used for the fuel used to climb to the cruise altitude,

$$W_{fclm} = C_{fclm} W_{to} \tag{20}$$

3.2 Aerodynamics

The aerodynamics technology for an aircraft is given by the drag polar:

$$C_{DCruise} = C_{Do} + C_{Dwave} + \frac{C_{LCruise}^2}{\pi AR\, E} \tag{21}$$

The subcritical zero lift drag coefficient is calculated from a skin friction analysis taking into account the fuselage, wing, vertical tail, and horizontal tail. A form drag coefficient is applied to the skin friction drag. Additional estimated zero lift drag contributions from the after-body drag, or boattail drag, engine pylon drag, and fuselage aft-end upsweep drag were also included.

$$C_{D_o} = C_{D_f} + C_{D_{Boat}} + C_{D_{Pylon}} + C_{D_{Upsweep}} \tag{22}$$

The friction drag, C_{D_f}, is given by,

$$C_{D_f} = \frac{\sum_{i=1}^{nc} \left\{ C_{f_i} \cdot C_{Form_i} \cdot S_{wet_i} \right\}}{S_{ref}} \tag{23}$$

where $C_{Form_{wing}}$ is the wing form drag coefficient found from the airfoil thickness at 75% of the span. Typical formulations of this coefficient for the wing can be found in reference 14. An example of this form drag coefficient for the wing is given by,

$$C_{Form_{Wing}} = 1 + 1.8(t/c_{75\%}) + 50(t/c_{75\%})^4 \tag{24}$$

The skin friction coefficient for each component is given by[15]

$$C_{f_i} = \frac{0.074}{\mathrm{Re}_i^{0.2}(1 + 0.144 M_\infty{}^2)} \tag{25}$$

which is adjusted for compressibility. Re is the Reynolds number based on the characteristic length of the particular component.

The transonic wave drag model is based on Lock's empirically based approximation[16],

$$C_{D_{wave}} = 20(M - M_{crit})^4 \tag{26}$$

which was recently derived theoretically by Inger[17]. When M is less than M_{crit}, the wave drag is zero. Using the definition of the drag divergence Mach number,

$$\frac{dC_{D_{wave}}}{dM} = 0.1 \tag{27}$$

M_{crit} can be found using Eqn (26) as,

$$M_{crit} = M_{DD} - \left\{\frac{0.1}{80}\right\}^{(1/3)} \tag{28}$$

The drag divergence Mach number was found using the Korn equation as extended to use sweep by Mason[9],

$$M_{DD} = \frac{\kappa_A}{\cos\Lambda} - \frac{(t/c)}{\cos^2\Lambda} - \frac{C_L}{10\cos^3\Lambda} \tag{29}$$

Here κ_a is a technology factor (range .87 to .95). This expression provides the relation between the lift, thickness and sweep for transonic drag rise. This expression also contains the effects of increasing takeoff weight through the cruise lift coefficient. This model was employed because of its ability to smoothly reflect the changing drag divergence Mach number during the design iterations.

Another model that could be used for the transonic drag rise is a two-piece linear fit. This method employs the use of a shallow linear fit from roughly 10% below M_{crit} to M_{DD} and a steeper fit from M_{DD} extrapolated upward. This method was originally used for the drag rise model, however, it was replaced with Lock's estimate as a result of the lack of smoothness at the drag divergence Mach number. The discontinuity in the gradient of the drag rise is not desirable in an optimization environment. Also, this method is not as easily adapted to changing critical Mach number.

The comparison of the predictions for both methods against data from ACSYNT is shown in Figure 2. We see that the linear fit is more accurate near M_{DD} , however,

Lock's fit smoothly models the transition at this point. Furthermore, Lock's fit becomes very accurate both below and above M_{DD}.

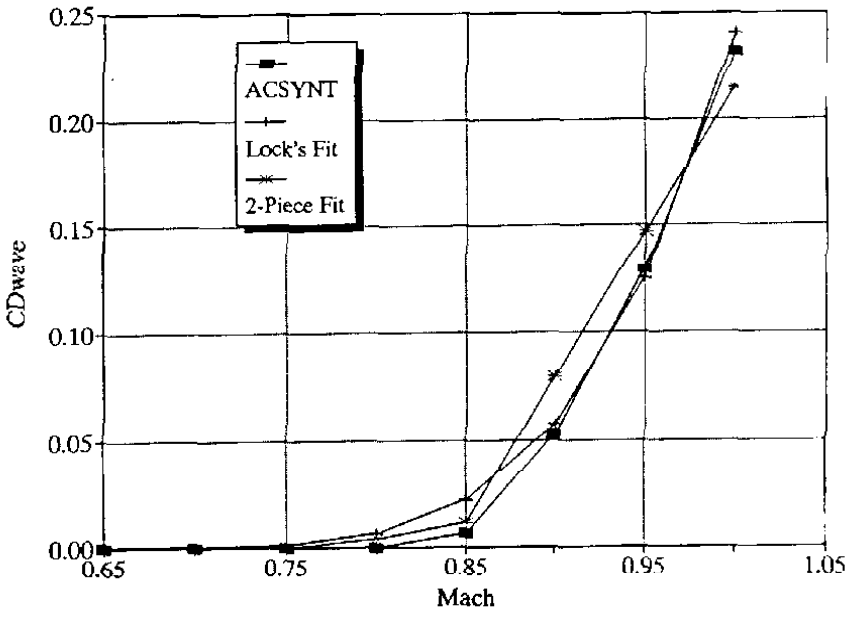

Figure 2. Wave Drag Model

The aerodynamic model also includes a constraint on C_L based on a prescribed limit section lift coefficient C_l. For this maximum section lift coefficient and assuming an elliptic spanload distribution, the total aircraft lift coefficient limit is given by,

$$C_{L_{Limit}} \leq \frac{\pi}{2} \cdot \frac{\sqrt{\lambda(2-\lambda)}}{(1+\lambda)} \cdot C_{l_{Limit}} \tag{30}$$

where λ is the taper ratio. This connects the section lift coefficient limit defined by the level of aerodynamic technology to the total aircraft lift limit. By imposing the

constraint as a function of a design variable, λ, the optimization can exploit the constraint limit to maximum advantage.

3.3 Performance

3.3.1.Takeoff

The takeoff distance, s, is given by finding a rotation velocity based on the takeoff weight and the field operations aerodynamics, then integrating over the velocity in the following equation.

$$s = \int_0^{V_{rot}} \left\{ \frac{W_{TO}}{g} \cdot \frac{v}{\{T_{\max} - Drag(v) - \mu(W_{TO} - Lift(v)\}} \right\} dv \tag{31}$$

Here, the rotation velocity is given by,

$$V_{rot} = \sqrt{\frac{2W_{TO}}{C_{L_{TO}} \cdot \rho \cdot S_W}} \tag{32}$$

Estimations of the distances covered during the rotation, transition and climbout are also included. These are simply empirical estimates of the time each of these phases require multiplied by the rotation velocity to give the distance. This model was based on the methods in Krenkel and Salzman[18].

3.3.2. Landing

Using the methods in Roskam[19], a model for analyzing the landing performance was developed. The method breaks the landing distance up into two segments, air distance, and ground roll.

The total landing distance is given by

$$S_{ldg} = S_{air} + S_{LG} \tag{33}$$

where S_{air} is the air distance from the point over a 50 ft obstacle to the touchdown point.

$$S_{air} = \frac{1}{\bar{\gamma}} \cdot \left\{ \frac{(V_a^2 - V_{Td}^2)}{2g} + h_l \right\} \tag{34}$$

Here, h_l is the height of the obstacle, and $\bar{\gamma}$ is the average aircraft drag-to-weight at landing, given by,

$$\bar{\gamma} = \left\{ \frac{(D-T)_{AVE}}{W} \right\} \tag{35}$$

and the touchdown velocity, V_{Td}, is defined by,

$$V_{Td} = V_a \sqrt{1 - \frac{\bar{\gamma}^2}{\Delta n}} \tag{36}$$

where the approach speed is typically taken to be 1.2 times the stall speed, found from the aircraft $C_{L_{max}}$ in the landing configuration,

$$V_a = 1.2 \cdot V_{stall} \tag{37}$$

The ground roll (S_{LG}) is estimated using a constant deceleration taking into account antiskid braking, thrust reversing, ground spoilers, and speed brakes. The thrust reversing model used assumes 40% of the maximum thrust available for the reversing system.

$$S_{LG} = \frac{V_{Td}^2}{2\bar{a}} \tag{38}$$

Here, $\bar{a}$ is the average deceleration. Although this is a conceptual level model, the results for landing analysis of similar transport class aircraft using this method as compared to published data are accurate to within 10%.

4. INTEGRATING THE TECHNOLOGY MODELS AS SUBSYSTEM VECTORS INTO THE GSE MATRIX

Each of the above technologies is considered analyses that contribute to the overall system. These technologies are represented by simple analytic expressions for the purpose of illustration. However, they could be large, complicated, and somewhat independent analysis routines that represent the most sophisticated computational methods for that discipline. The key is the relationship between the input and the output information required for these technologies, and what each technology requires in terms of system information (i.e. design variables).

To properly capture the relationships between disciplines, the Global Sensitivity Equations must be written in the format described in Eqn. (10). This requires the selection of the most important outputs from each discipline. The selection must be made carefully, however, so that the order of the GSE matrix is kept low, and thus the gradients can be computed quickly. If non-coupled outputs, those that have little or no effect on the overall system, are selected, the GSE matrix becomes unnecessarily large, and the solution to find the system gradients at each iteration in the optimization process becomes expensive computationally.

The coupling effects between weights and aerodynamic performance at the conceptual aircraft sizing level were the main interactions desired in this research. It became obvious that the aerodynamics discipline output vector should include the cruise performance parameters, along with the critical field performance parameters. The weights discipline vector was simply the component weights.

It was found that W_{to} was required to be grouped separately from the other weights because of the dependence on the component weights. Even though the takeoff weight is simply the sum of the component weights, it is a separate subsystem because it must

have the coupling effects of those components. The takeoff weight is coupled to the components weight in the most basic forms because it is simply a linear combination of the components. The nature of the process requires that the disciplines be treated as analysis that depend on only the design variable set and the outputs of the other disciplines. It is crucial, therefore, that not only are the proper discipline outputs chosen, but the proper disciplines themselves.

Thus, the technologies were placed in three separate subsystems for use in the calculation of the global sensitivities. The contents of each subsystem vector are:

$$\mathbf{Y}_{Aero} = \begin{Bmatrix} C_{L_{Cruise}} \\ V_{rot} \\ C_{D_{Cruise}} \\ S_{to} \\ S_{ldg} \end{Bmatrix} \qquad \mathbf{Y}_{Weights} = \begin{Bmatrix} W_{fuel} \\ W_{wing} \\ W_{eng} \\ W_{fix} \\ W_{fclm} \\ W_{cargo} \end{Bmatrix} \qquad \mathbf{Y}_{Wto} = \{W_{to}\} \tag{39}$$

5. THE OPTIMIZATION PROBLEM

5.1 Problem Statement

It is important to properly define the optimization problem and the constraints before the computation of the solution is started. Traditionally, the aircraft designer chooses to minimize the takeoff gross weight of the aircraft. This has several benefits. First, W_{to} is related to the cost of the aircraft. Secondly, W_{to} is a measure of the cruise performance. A heavy aircraft is an indication of large fuel weights, i.e. higher required thrust, hence, poor cruise performance. Finally, the field performance is closely coupled with the takeoff weight. A heavier aircraft requires a longer takeoff distance. There are benefits to choosing other figures of merit[20], as will be discussed later. However, for the current optimization statement, we chose the takeoff gross weight as the figure of merit.

With the proper objective function selected, and suitable constraints chosen, the appropriate optimization problem statement can be given by,

$$\begin{aligned} &\min f(x) && x \in \Re^n \\ &g_j(x) = 0, && j = 1,\ldots,m_e, \\ &g_i(x) \geq 0, && i = m_e+1,\ldots,m \\ &x_l \leq x \leq x_u \end{aligned} \tag{40}$$

Where $f(\mathbf{x})$ is the objective function, taken here to be the takeoff weight, and $g(x)$ is the set of constraints imposed on the system. According to appropriate technology limitations in the field of structures and aerodynamics, suitable lower (x_l) and upper (x_u) bounds were placed on the design variables.

The takeoff gross weight was selected as the objective function for the optimization problem, although any of the components (or a combination) of the **Y**'s can be selected as the figure of merit. In addition to the objective function, the constraints chosen were the takeoff distance and the attainable section lift coefficient in the cruise phase, as discussed previously.

5.2 Design Variable Set

The design variables were chosen to include both aircraft geometry and flight performance values. Seven design variables were chosen as a representative set available for optimization:

$$\mathbf{X} = \begin{Bmatrix} AR \\ S_w \\ h \\ M \\ \Lambda \\ t/c \\ \lambda \end{Bmatrix} \tag{41}$$

5.3 Baseline Configuration

An example was selected to illustrate the method. In this case, a short takeoff, medium range heavy transport was used. Table 1. shows the specified mission along with a suitable candidate for the propulsion system. For this example, the range was fixed, along with the engine thrust.

Table 1. Mission Requirements/Constraints

Cargo Weight	150,000 lbs
Range	3000 nm
Takeoff Distance	5000 ft
Landing Distance	4000 ft
Maximum C_L	2.3
Maximum Section C_l	1.0
Propulsion	4 CF6 class Turbofans ($T/W_{eng} = 6$)

Although not necessary, ACSYNT was used to establish a baseline model from the data. Because ACSYNT is a fully developed and well tested sizing software package, it was used not only for the baseline estimates, but also as a comparison code throughout the development of the multidisciplinary process. An ACSYNT input file was created using published data for similar aircraft[21]. A mission profile was specified for the candidate aircraft based on a 3000 nm cruise range. This cruise range accounted for the base mission range plus an extra distance to account for reserve fuel requirements. The given initial estimates for the takeoff gross weight and fuel weight came from this analysis. ACSYNT also gave estimates of the zero lift drag that were used to verify the analytic aerodynamic models.

Because the individual disciplines are actually sets of nonlinear, coupled equations (Sobieski[4]), a solution to these equations must be obtained initially before the global sensitivity equations can be calculated. This coupling is evident in the relationship between the wing weight and the gross weight. The wing weight is a function of the

gross weight, which is a function of the wing weight. Fixed point iteration was used to converge the set of equations for a given cruise range and set of design variables.

5.4 Solving the Global Sensitivity Equations

Once the subsystems were defined in terms of the technology models, and all the discipline interactions calculated in the GSE matrix, the global derivatives were computed. Table 2. shows the actual GSE matrix that was computed for the baseline aircraft. The shaded portions of the matrix illustrate the structure and the relative sizes of each analytic subsystem used for this example. Table 3. shows the local and global derivatives, as described above. Notice that the local gradient of W_{to} is zero for every design variable. This comes from the formulation of the takeoff gross weight as a separate subsystem. As specified, the **Y3** subsystem does not have design variables explicitly in the formulation, rather, it is simply the sum of the elements in the **Y2** discipline (the component weights). As a result, when a derivative of W_{to} with respect to any of the design variables is computed using finite differencing on that discipline alone, the gradient is zero. When the interactions of the aerodynamics and component weights subsystems are taken into account, however, the resulting global derivatives then reflect the actual function gradient.

Table 2. Actual Partitioned GSE Matrix for 3 Subsystem Design Problem.

Global Sensitivity Matrix												
	CL	*Vrot*	*CD*	*Sto*	*Sldg*	*Wfuel*	*Wwing*	*Weng*	*Wfclm*	*Wfix*	*Wcargo*	*Wto*
CL	1.0000	0.0000	0.0000	0.0000	0.0000	0.0000	0.0000	0.0000	0.0000	0.0204	0.0000	-1.0204
Vrot	0.0000	1.0000	0.0000	0.0000	0.0000	0.0000	0.0000	0.0000	0.0000	0.0000	0.0000	-0.4969
CD	0.0000	0.0000	1.0000	0.0000	0.0000	0.0000	0.0000	0.0000	0.0000	0.0289	0.0000	-1.4581
Sto	0.0000	0.0000	0.0000	1.0000	0.0000	0.0000	0.0000	0.0000	0.0000	0.0000	0.0000	-1.7383
Sldg	0.0000	0.0000	0.0000	0.0000	1.0000	0.1375	0.0000	0.0000	0.0000	0.0000	0.0000	-0.9514
Wfuel	0.8185	0.0000	-0.8318	0.0000	0.0000	1.0000	0.0000	0.0000	0.0000	0.0000	0.0000	-1.0000
Wwing	0.0000	0.0000	0.0000	0.0000	0.0000	0.0000	1.0000	0.0000	0.0000	0.0000	0.0000	-0.8383
Weng	0.0000	0.0000	0.0000	0.0000	0.0000	0.0000	0.0000	1.0000	0.0000	0.0000	0.0000	0.0000
Wfclm	0.0000	0.0000	0.0000	0.0000	0.0000	0.0000	0.0000	0.0000	1.0000	0.0000	0.0000	-1.0000
Wfix	0.0000	0.0000	0.0000	0.0000	0.0000	0.0000	0.0000	0.0000	0.0000	1.0000	0.0000	-1.0000
Wcargo	0.0000	0.0000	0.0000	0.0000	0.0000	0.0000	0.0000	0.0000	0.0000	0.0000	1.0000	0.0000
Wto	0.0000	0.0000	0.0000	0.0000	0.0000	-0.2891	-0.0956	-0.0473	-0.2950	-0.0200	-0.2531	1.0000

Table 3. Local and Global Sensitivities

Local Derivatives								Global Derivatives						
Ar	*Sw*	*Alt*	*Mach*	*Sweep*	*t/c*	*Taper*		*Ar*	*Sw*	*Alt*	*Mach*	*Sweep*	*t/c*	*Taper*
0.0000	-0.9756	1.5205	-1.9274	0.0000	0.0000	0.0000	*CL*	-0.1609	-1.2263	2.2503	1.4592	-0.2556	0.2127	0.0634
0.0000	-0.4908	0.0000	0.0000	0.0000	0.0000	0.0000	*Vrot*	-0.0800	-0.6154	0.3627	1.6828	-0.1270	0.1057	0.0315
-0.5372	-1.3673	2.1832	0.6591	-0.3121	0.4803	0.0000	*CD*	-0.7672	-1.7256	3.2263	5.4994	-0.6774	0.7842	0.0906
-0.0996	-0.9278	0.0000	0.0000	0.0000	0.0000	0.0000	*Sto*	-0.3794	-1.3636	1.2688	5.8870	-0.4442	0.3697	0.1102
0.0000	-0.7941	0.0000	0.0000	0.0000	0.0000	0.0000	*Sldg*	-0.0613	-0.9388	0.4844	2.2476	-0.1593	0.1073	0.0484
0.0000	0.0000	-0.0442	0.3203	0.0000	0.0000	0.0000	*Wfuel*	-0.6673	-0.6823	1.5273	7.0868	-0.6098	0.6909	0.0869
1.0000	0.4769	0.0000	0.0000	0.2269	-0.7437	0.1385	*Wwing*	0.8651	0.2668	0.6119	2.8391	0.0127	-0.5654	0.1917
0.0000	0.0000	0.0000	0.0000	0.0000	0.0000	0.0000	*Weng*	0.0000	0.0000	0.0000	0.0000	0.0000	0.0000	0.0000
0.0000	0.0000	0.0000	0.0000	0.0000	0.0000	0.0000	*Wfclm*	-0.1609	-0.2507	0.7299	3.3866	-0.2556	0.2127	0.0634
0.0000	0.0000	0.0000	0.0000	0.0000	0.0000	0.0000	*Wfix*	-0.1609	-0.2507	0.7299	3.3866	-0.2556	0.2127	0.0634
0.0000	0.0000	0.0000	0.0000	0.0000	0.0000	0.0000	*Wcargo*	0.0000	0.0000	0.0000	0.0000	0.0000	0.0000	0.0000
0.0000	0.0000	0.0000	0.0000	0.0000	0.0000	0.0000	*Wto*	-0.1609	-0.2507	0.7299	3.3866	-0.2556	0.2127	0.0634

5.5 Sequential Quadratic Programming (NLPQL Routine)

The optimization was performed using NLPQL[22], a FORTRAN implementation of a sequential quadratic programming (SQP) method for solving nonlinearly constrained optimization problems. At each iteration, the search direction is a solution of a quadratic programming subproblem. NLPQL uses gradients of the objective function and the constraint functions obtained from the solution of the global sensitivities as described in Eqn (10).

The underlying methodology of the SQP algorithm is the formulation of a quadratic subproblem. A brief description of the problem and the main assumptions follows.

Let x_k be the current iterate, v_k, the approximation of the optimal Lagrange multipliers, and $\mathbf{B_k}$ a positive definite approximation of the Hessian matrix of the Lagrange function. Then, we can write the Lagrangian function in the following manner,

$$L(x,u) = f(x) - \sum_{j=1}^{m'} u_j g_i(x) \tag{42}$$

where $x \in \Re^n$, $u = (u_1, \cdots, u_{m'})^T \in \Re^{m'}$ and m' is defined as $(m+2n)$. We can also define the constraint functions as,

$$\begin{aligned} g_j(x) &= x^{(j-m)} - x_l{}^{(j-m)} && j = m+1, \ldots, m+n \\ g_i(x) &= x_u{}^{(i-m-n)} - x^{(i-m-n)} && i = m+n+1, \ldots, m' \end{aligned} \tag{43}$$

When the constraints from the original optimization problem posed in Eqn. (40) are linearized, and the approximation to the Lagrangian function (42) is posed as a minimization problem, we have the following subproblem,

$$\begin{aligned} &\min \frac{1}{2} d^T \mathbf{B_k} d + \nabla f(x_k)^T d \\ &\nabla g_j(x_k)^T d + g_j(x_k) = 0 \qquad j = 1, \ldots, m_e, \\ &\nabla g_i(x_k)^T d + g_i(x_k) \geq 0 \qquad i = m_e + 1, \ldots, m \\ &d \in \Re^n \qquad x_l - x_k \leq d \leq x_u - x_k \end{aligned} \tag{44}$$

If d_k is the solution to the above subproblem, and u_k is the vector of Lagrange multipliers, then the new iterate is defined by,

$$x_{k+1} = x_k + \alpha_k d_k \tag{45}$$

where α_k is the steplength parameter, found to satisfy a sufficient decrease in a given merit function,

$$\varphi(\alpha) = \psi_{r_k} \left(\begin{Bmatrix} x_k \\ v_k \end{Bmatrix} + \alpha \begin{Bmatrix} d_k \\ u_k - v_k \end{Bmatrix} \right) \tag{46}$$

6. DESIGN VARIABLE SENSITIVITIES

Before a complete optimization of the baseline aircraft was carried out, each design variable was examined to study typical sensitivity of the objective function. Because the direction each design variable will take is not known in the full optimization, by first examining the individual parametrics, the final solution to the completely optimized aircraft will provide greater insight. Four of the seven design variables along with the GSE derivatives computed using the methods described previously, are examined in Figure 3.1- 3.4.

6.1 Aspect Ratio

Over the range of aspect ratio, with all other design variables fixed, there exists a *minimum* weight value of AR. The computed derivative from the GSE method accurately captures the minimum point as the derivative passes through zero.

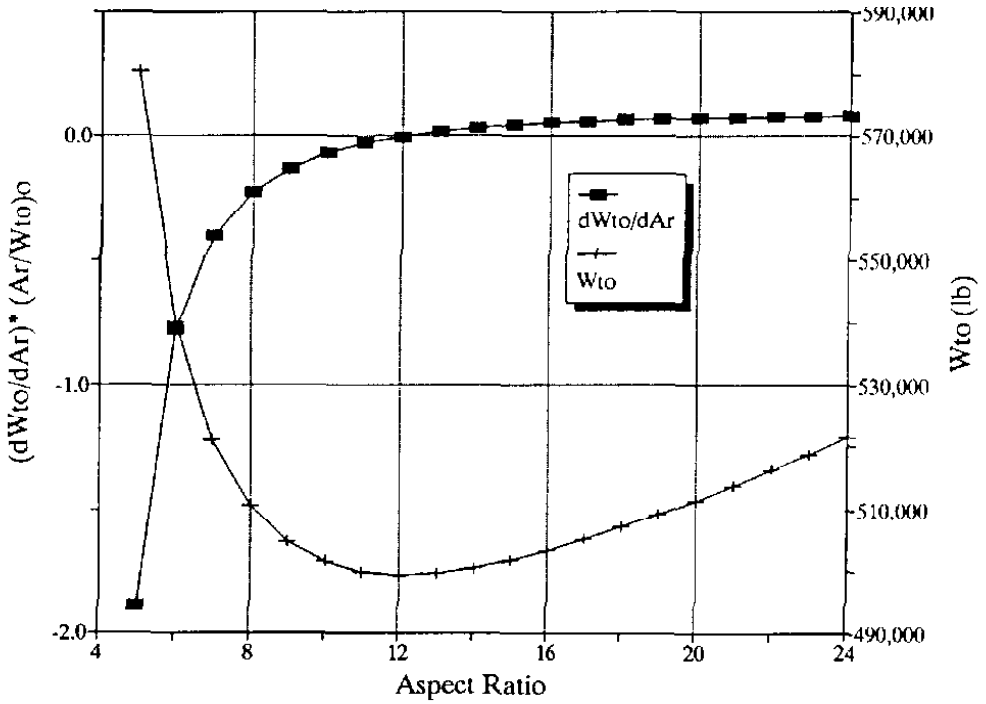

Figure 3.1 Aspect Ratio Sensitivity.

6.2 Wing Area

We can see from the computed derivative that the minimum weight wing area for this range, all other variables fixed, lies close to the selected lower bound. As the wing continues to grow, the structural weight begins to increase. With increasing wing area, however, the fuel weight decreases. A larger wing allows for a smaller cruise C_L and thus a smaller C_D.

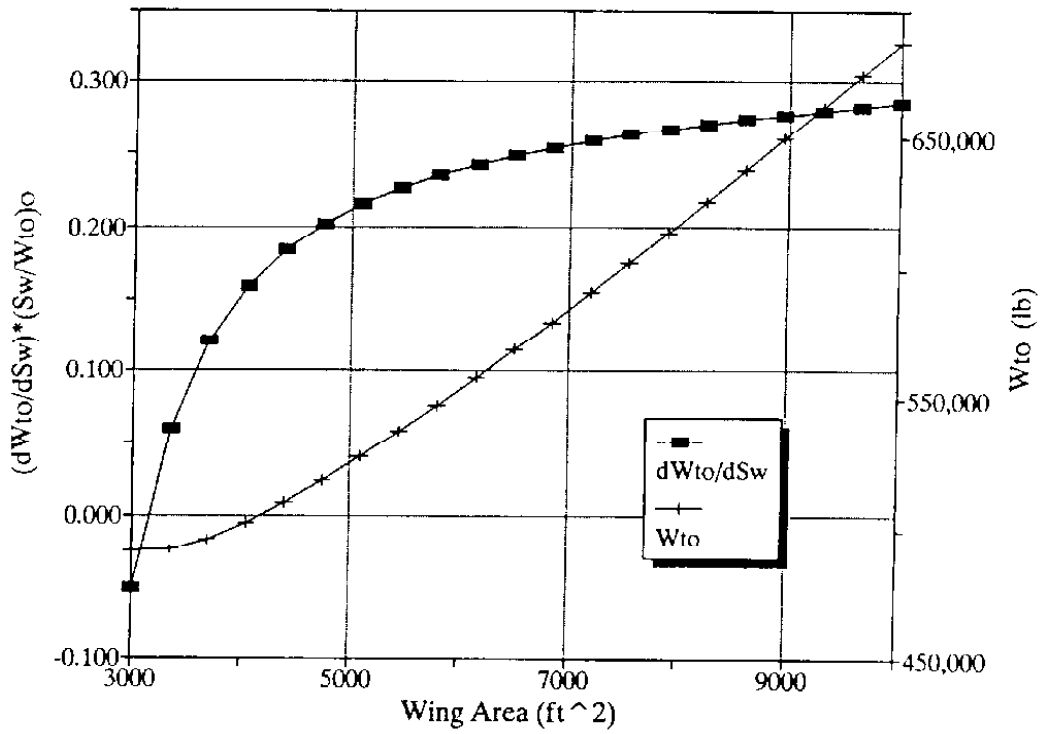

Figure 3.2 Wing Area Sensitivity.

6.3 Wing Sweep

The objective function for a range of wing sweeps shows that at a fixed Mach number sweep is necessary to alleviate the effects of the transonic drag rise. However, as the wing is swept beyond what is needed, the penalty of the structural weight begins to exceed the payoffs from the transonic drag reduction. The minimum weight solution

exhibited in the sweep parametric is highly dependent on the cruise Mach number that is specified. For the case shown, the cruise Mach number was .78 and the resulting optimum sweep was 30 deg. For lower Mach numbers, the minimum weight solution would be found at lower wing sweeps.

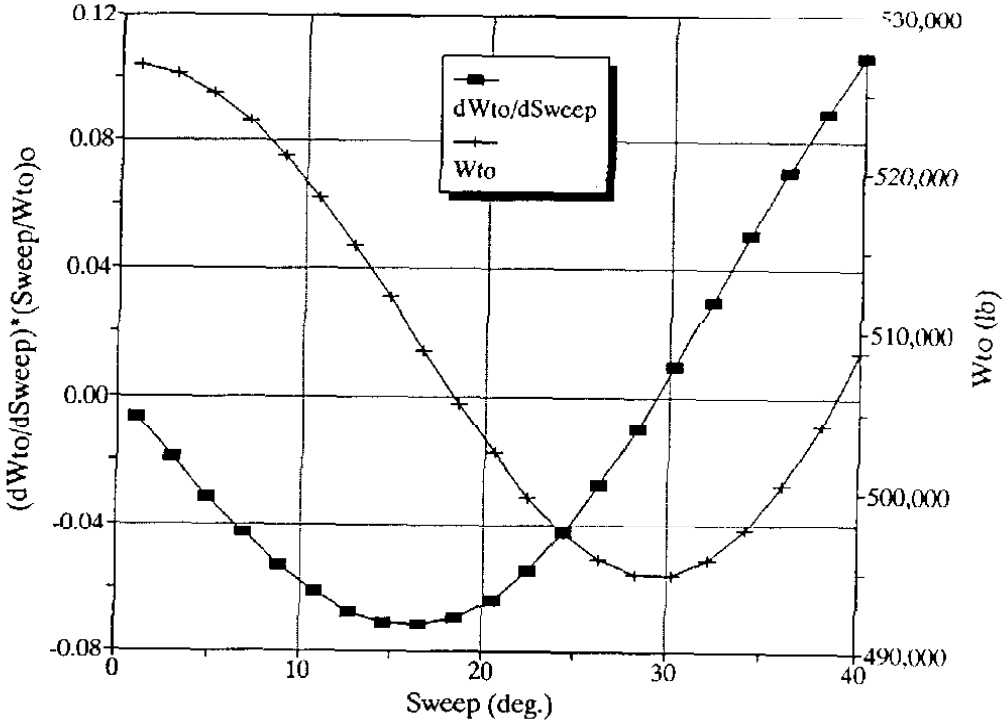

Figure 3.3 Sweep Sensitivity.

6.4 Mach Number

The behavior of W_{to} with Mach number shows limitations both at low and high Mach numbers. The high Mach limitations are a result of the transonic drag rise, whereas the low Mach number limitations can be explained by examining the range factor,

$$\frac{M(L/D)}{sfc} \tag{47}$$

At Mach numbers below 0.55, the cruise performance is greatly affected by poor lift to drag ratios, for a fixed altitude, as well as the reduced speed.

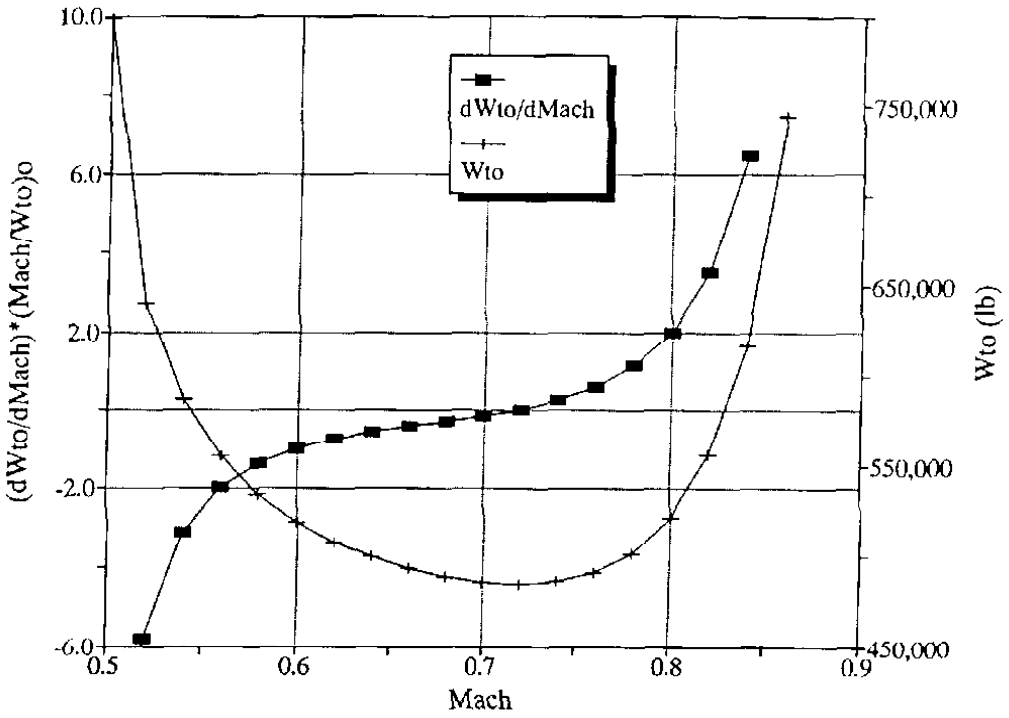

Figure 3.4 Cruise Mach Number Sensitivity.

7. RESULTS

In order to compute the subsystem coupling effects in the sizing process, a computer code was written to incorporate the technology models into the GSE structure. This code has the capability to run many different cases ranging from simple analysis to complete optimization. See the Appendix for a complete description of the code.

7.1 Full Set Optimization

Using the analytic models for the technology, many (hundreds) of optimization cases can be computed. For the general case, Table 4. shows the design variables, objective function, and constraints before and after the optimization. Figure 4. shows the convergence history for the optimization using all seven design variables. Note that even though the weight is nearly converged at 17 iterations, the design variables are still changing until 24 iterations.

Table 4. Initial Point vs. Optimized Solution.

	Initial	*Final*
Aspect Ratio	7.00	22.65
Wing Area (ft^2)	3800	3957
Cruise Altitude (ft)	39,600	35,936
Mach Number	0.78	0.61
Mid-Chord Sweep (deg.)	21.0	1.0
Thickness Ratio (t/c)	.10	.18
Taper Ratio	.10	.27

Takeoff distance (ft)	6301	5000
Landing distance (ft)	2713	2355
Cruise C_L	.8431	.9621
Cruise C_D	.0714	.0400
-Weights-		
Fuel (lb)	167,677	96,614
Wing (lb)	50,771	64,512
Engine (lb)	30,000	30,000
Fixed (lb)	136,455	116,824
Climb Fuel (lb)	10,916	9,345
Cargo (lb)	150,000	150,000
Gross Weight (lb)	545,820	467,298

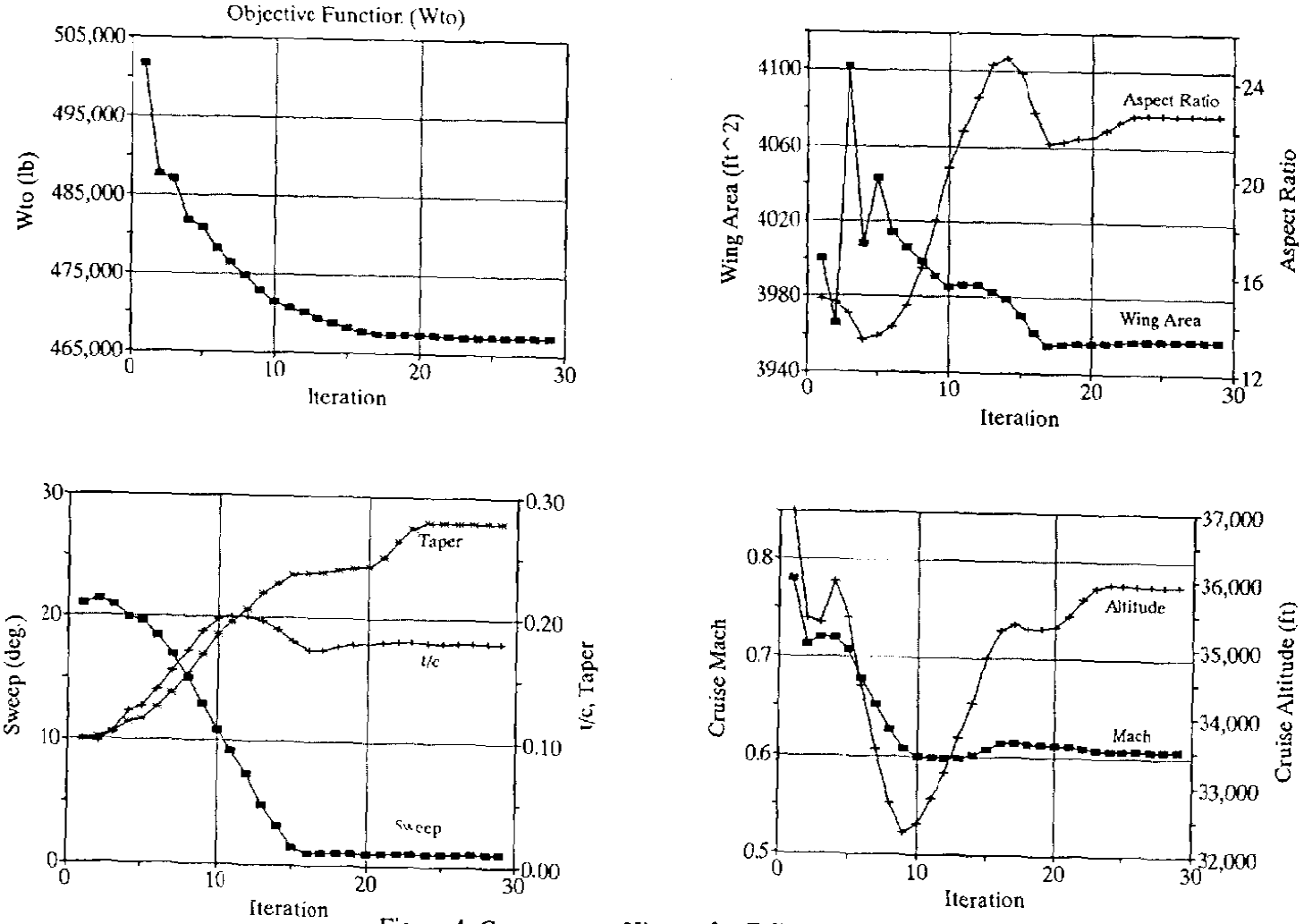

Figure 4. Convergence History for Full Design Set.

Table 4. shows how the optimization process results in a low speed (M=0.61) design when all of the design variables are available to the optimization. The objective function was reduced by 15%, and the results shifted from a moderately swept design to that of a high aspect ratio, no-sweep design. The high aspect ratio is a result of a reduced penalty in the wing weight equation. The validity of the wing weight equation becomes questionable at this aspect ratio. This design also has a high cruise lift coefficient (0.9621) however, the cruise drag was reduced 44%. The section lift coefficient limit was 1.0 for this case.

7.2 Optimized Solutions For a Range of Mach Numbers

The results shown in Figure 4. give information for one design. Much more insight can be obtained by examining optimum results over the range of a specified parameter. Mach number is a good example. The effect of a mission-specified Mach number, as would be given in a typical design request for proposal, can be observed by fixing the Mach number and optimizing the aircraft with respect to the reduced design variable set. By implementing the optimization in this manner, we can easily identify the tradeoffs of performance, aerodynamics, and structures as the wing evolves from a low speed design to a high-speed, transonic design.

Figure 5. shows a range of optimal solutions for a specified Mach number from 0.5 to 0.9. The first set of results shows the effect of imposing only the takeoff constraint ($S_{to} \leq 5000.0$ ft), whereas the second set includes the takeoff constraint as well as the section lift coefficient constraint ($C_l = 1.0$).

The optimal solution presented in Table 4. is shown as the minimum of the W_{to} plot in Figure 5. Note that increasing Mach number results in an increased weight, and wing area. The results show a decreasing aspect ratio as the wing area is sized for the

takeoff constraint. At low Mach numbers, the wing is unswept, but as the cruise Mach number is increased, the sweep begins to increase abruptly, as the wing requires more and more sweep to alleviate the transonic drag effects. This sudden increase in sweep was unexpected. However, it can be compared to the sweep schedule that is used for a variable sweep wing aircraft such as the F-14, as shown in Figure 6., taken from the paper by Kress[23]. From a structural standpoint, the wing thickness is optimal at large values, however, aerodynamically, a thick wing creates increased form and wave drag.

The effect of adding the C_l constraint is reflected in the taper ratio. For the first case, the taper ratio is reduced to the imposed lower bounds in order to reduce the wing weight. In the second case, however, the constraint limit imposed on the aircraft lift coefficient is a function of the taper ratio, therefore the addition of the C_l constraint illustrates how the taper ratio is now used to reduce the constraint limit value.

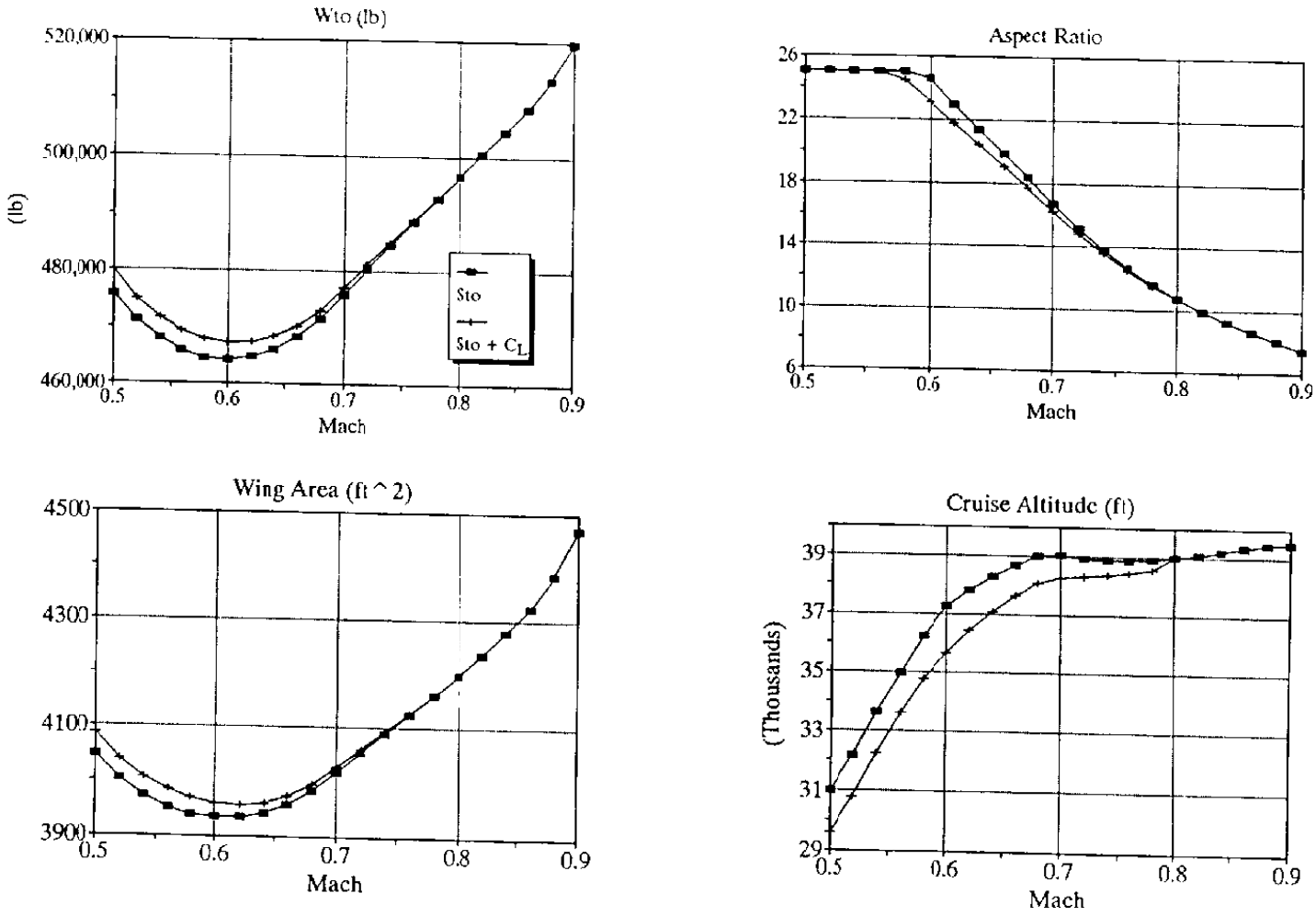

Figure 5. Optimal Solutions for a Range of Specified Mach Numbers.

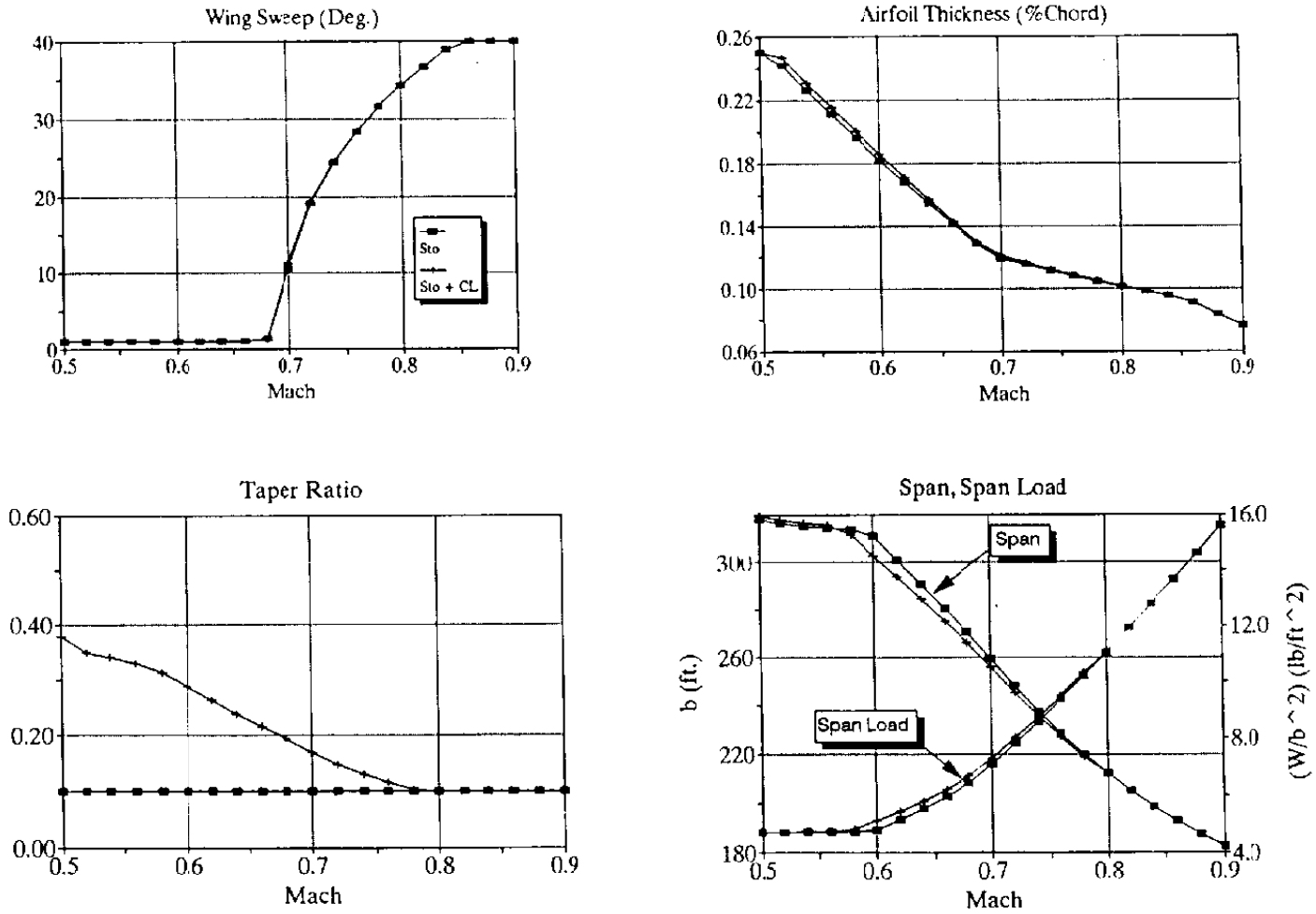

Figure 5. (Continued) Optimal Solutions for a Range of Specified Mach Numbers.

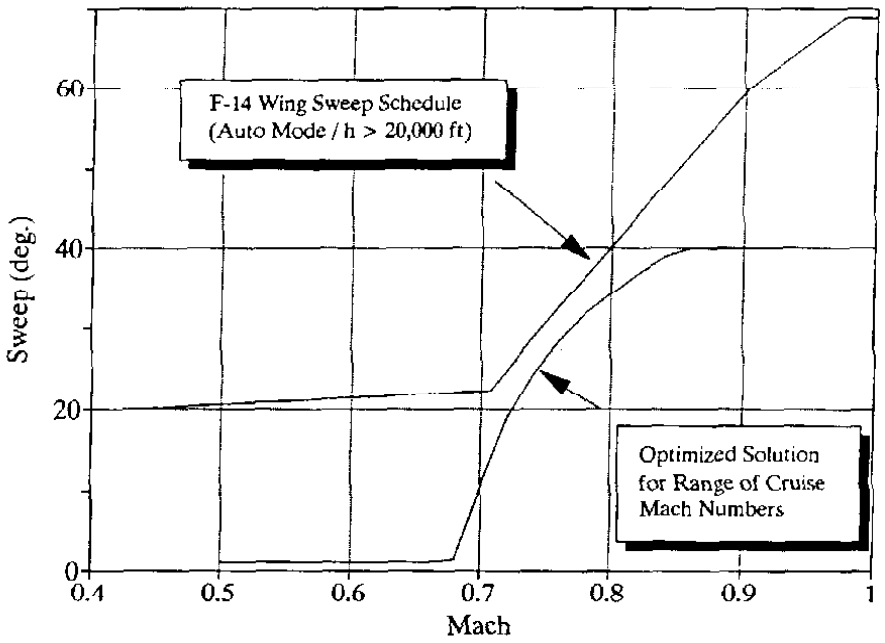

Figure 6. F-14 Wing Sweep Schedule.

7.2.1 Planforms for Range of Mach Numbers.

Figure 7. shows the geometry of the design variables in the form of planform plots. We see that for the low Mach numbers the sweep is reduced to its lower limit, but more striking is the increase in span over the baseline design. Also visible is the dramatic sweep effect as the Mach number is increased. The reduction of the aspect ratio is evident as the span is reduced at M=0.9 to nearly half that of the M=0.5 solution. These results are for the takeoff constraint only case.

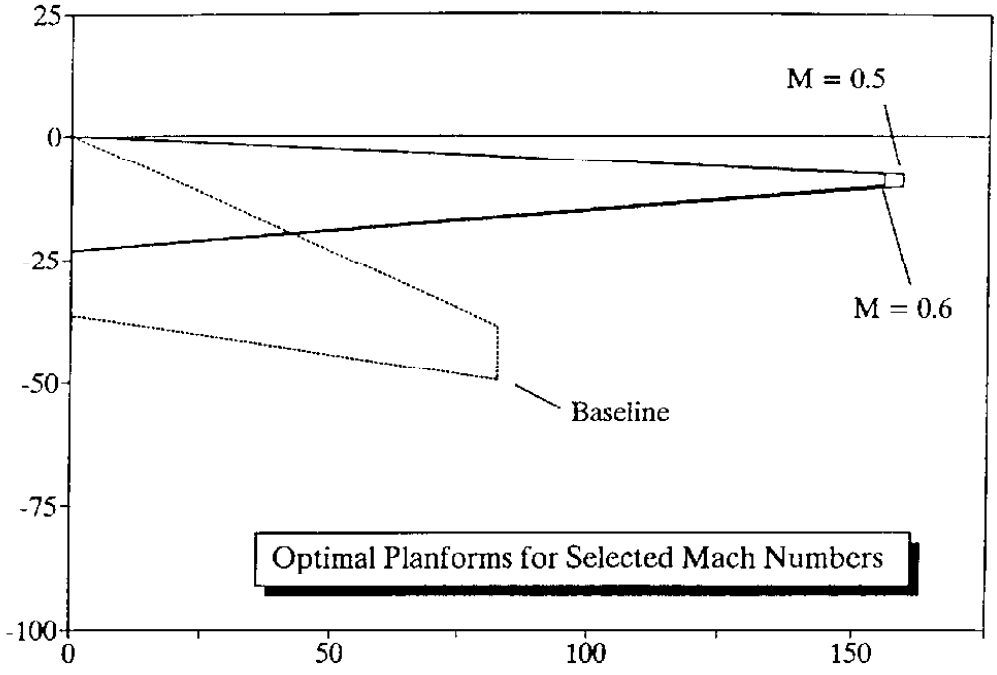

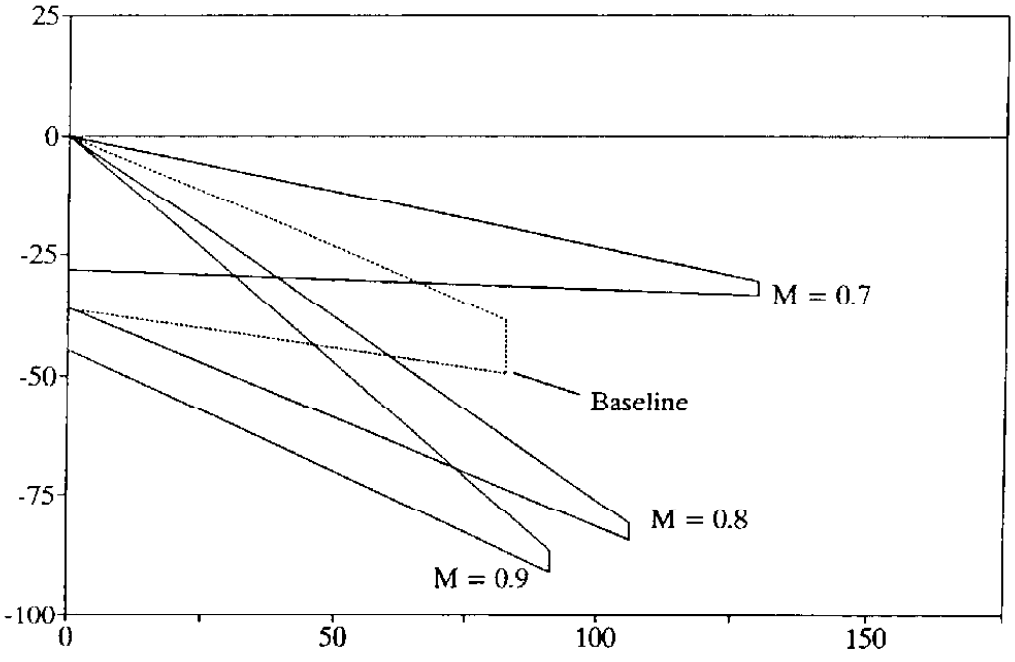

Figure 7. Planforms for Selected Cruise Mach Numbers.

7.3 Effect of Cruise Range

The effect of range on the design is shown in Figures 8.1-8.3. As the range is increased from 2000 nm. to 3000 nm, the takeoff weight increases by 80,000 lb. Note that as the range is increased, the emphasis shifts from a structurally biased design (low AR) to that of an aerodynamically biased design (high AR). The C_L is at the imposed constraint limits, however, the lift to drag ratio is increasing as the aircraft is gaining necessary efficiency to achieve the longer range. This case was for a Mach number of 0.78.

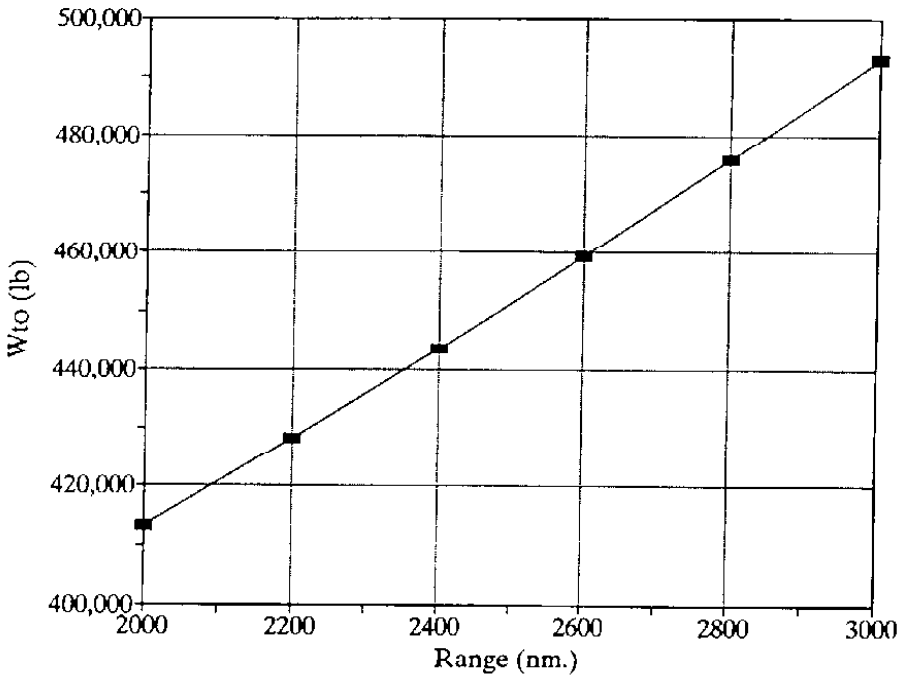

Figure 8.1 Effect of Cruise Range on Optimum: Objective Function. (M=0.78)

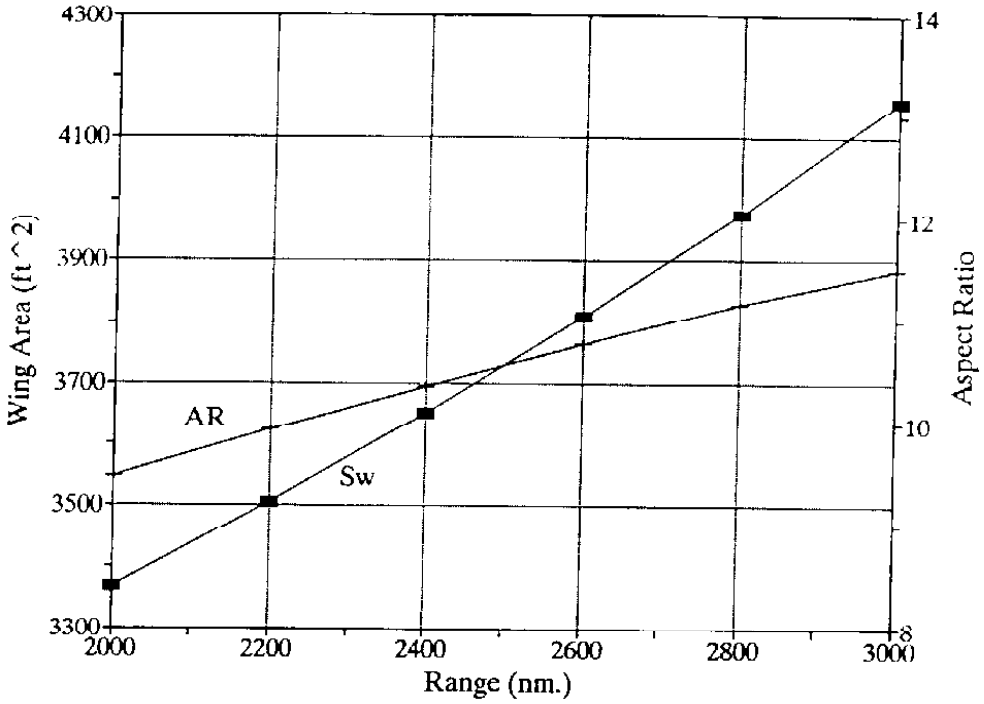

Figure 8.2 Effect of Cruise Range on Optimum: Wing Area / Aspect Ratio. (M=0.78)

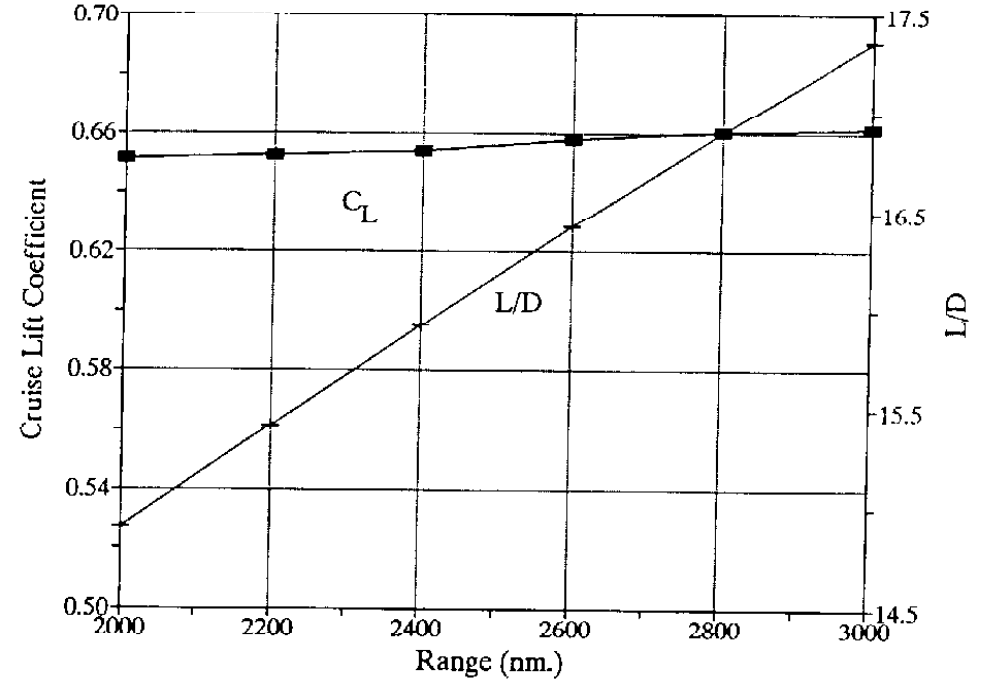

Figure 8.3 Effect of Cruise Range on Optimum: Aerodynamic Performance. (M=0.78)

7.4 Effect of Takeoff Constraint

Figures 9.1-9.3 show the large penalty in weight due to the effect of the takeoff constraint on the optimum solution. This case was also optimized for a fixed Mach number of 0.78. For very short takeoff distances, the wing area becomes very large. In contrast to Figure 8, the L/D is relatively unchanged, however, the cruise C_L is greatly reduced at the short takeoff distances due to the large wing. Also, because the wing area is so large at the short takeoff constraints, the aspect ratio is reduced greatly. This is caused by the penalty incurred in the wing weight equation for large spans.

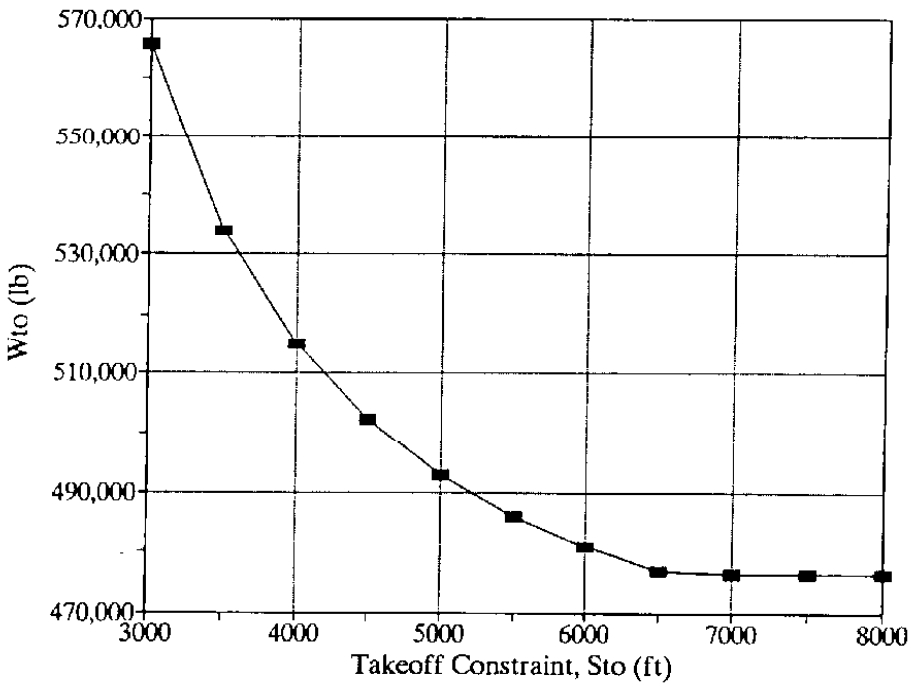

Figure 9.1 Effect of Takeoff Constraint: Objective Function.

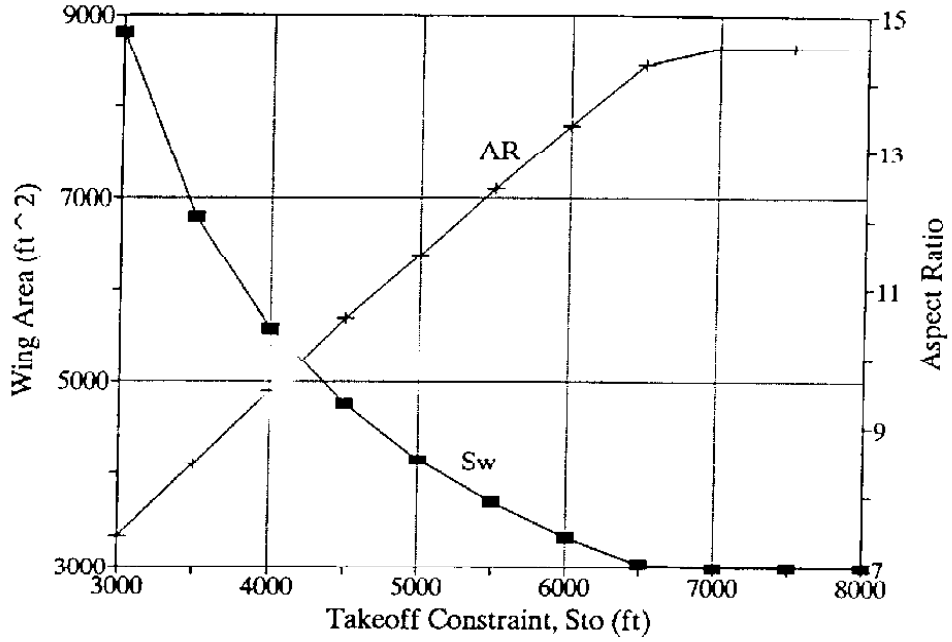

Figure 9.2 Effect of Takeoff Constraint: Wing Area / Aspect Ratio.

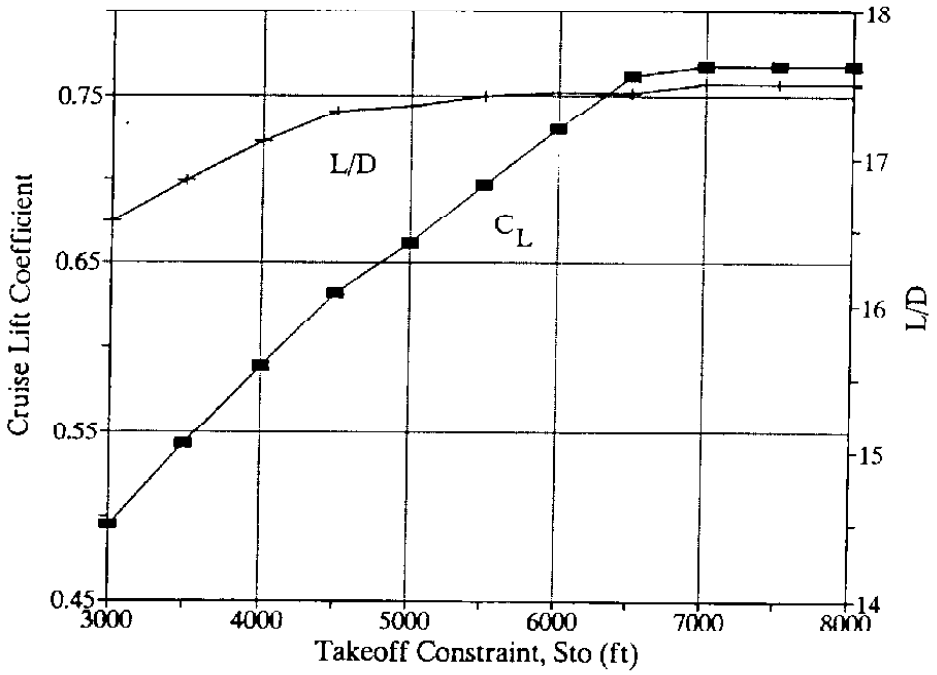

Figure 9.3 Effect of Takeoff Constraint: Aerodynamic Performance.

7.5 Effect of Limited Design Variable Set

Insight can also be gained by examining the effect of different design variables on the optimum.

7.5.1 Case 1.

The design variables were limited to:

$$\mathbf{X} = (Ar, Sw)^T \tag{48}$$

All other design variables were held constant at their baseline values and the cruise Mach number was varied parametrically. The constraint limit placed on the takeoff distance was 5000 ft. and the section cruise C_l limit was 1.0. The numerical results in Figure 10. show a decrease in the aspect ratio with increasing Mach. The wing area decreased to a point where the takeoff constraint became active, then remained at the required wing loading to minimize the design while remaining within the feasible design region. For this limited design variable case, the optimum solution is found at a Mach number of 0.73.

7.5.2 Case 2.

The design variable set was expanded to the following,

$$\mathbf{X} = (Ar, Sw, \Lambda)^T \tag{49}$$

The minimum now occurs for M=0.6. The aspect ratio result shows the effect of the wing area being sized by the takeoff constraint. At that point, the wing area began decreasing

to account for the affected cruise performance. As expected, to alleviate the transonic drag, the optimum wing sweep increases with increasing Mach number.

7.5.3 Case 3.

$$X = (Ar, Sw, \Lambda, t/c)^T \tag{50}$$

By adding the airfoil thickness into the set of design variables, several interesting results occur. First, there is an obvious shift in technology focus from an aerodynamic design, as shown in cases 1 and 2, to a structural design. By using thickness as a design variable, the optimum solutions found at low Mach numbers reflect a very high aspect ratio. This is a direct result of the structural wing weight equation. As the thickness is allowed to increase above the baseline, the wing becomes lighter, thus allowing the higher aspect ratio designs to become more feasible. However, aerodynamically, the wing sweep plot shows that with a thicker wing, more sweep is needed at a given Mach number to account for the increased transonic drag.

7.5.4 Case 4.

Finally, the design was optimized for a range of Mach numbers using the variable set used in Figure 4.

$$\mathbf{X} = (Ar, Sw, h, \Lambda, t/c, \lambda)^T \tag{51}$$

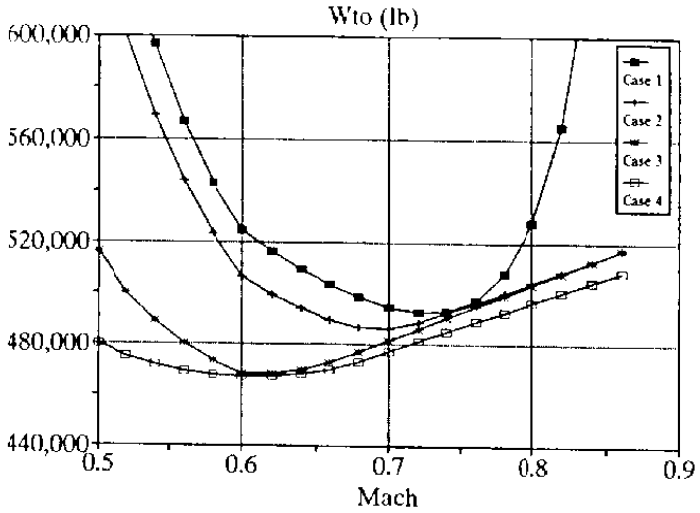

Case 1. X = {AR, Sw}

Case 2. X = {AR, Sw, Sweep}

Case 3. X = {AR, Sw, Sweep, t/c}

Case 4. X = {AR, Sw, Sweep, t/c, taper, h}

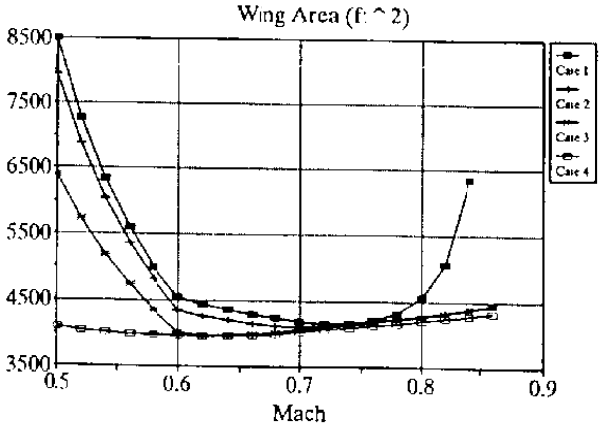

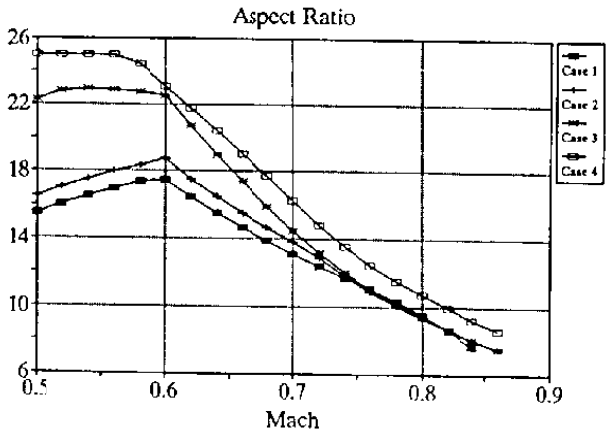

Figure 10. Effect of Design Variable set.

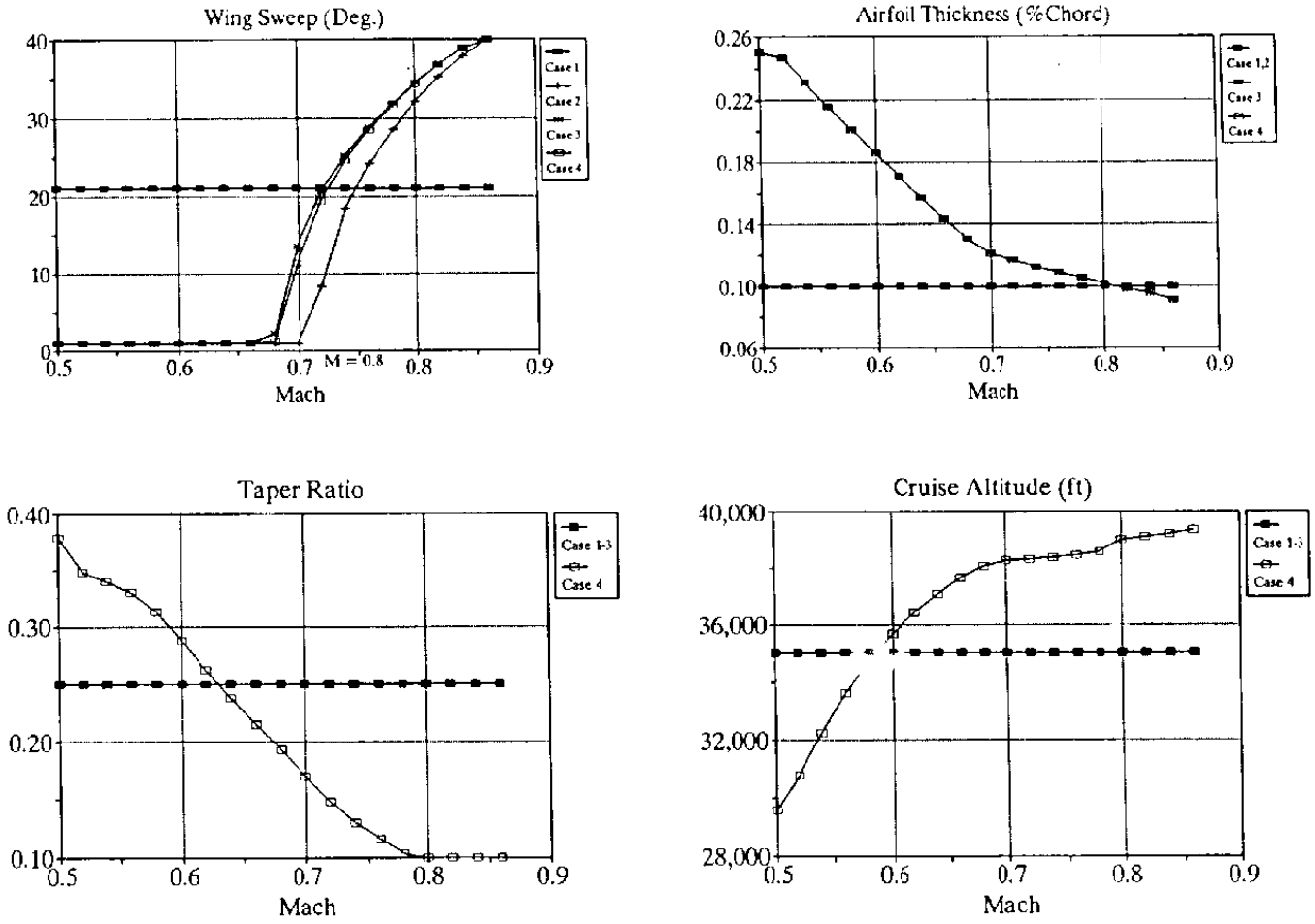

Figure 10. (Continued) Effect of Design Variable set.

8. DEMONSTRATION OF INCREASED TECHNOLOGY COMPLEXITY

8.1 Second Order Effects of Several Wing Weight Equations

Aircraft conceptual design is not an exact sport. The process of collecting empirical data to establish a database of aircraft design variable trends leads to weight equations that, on the first order, produce fairly accurate results. But, as the second order effects are called upon by an optimization routine, these equations can produce strikingly different results.

For example, in the sizing of an aircraft wing for a cruise dominated mission, the wing weight equation plays a crucial role. A required level of field performance that must be met is usually coupled with a long range cruise specification. The optimization process is confronted with a conflicting set of constraints, for as the wing area is increased to enhance the field performance, the takeoff gross weight is compromised with the increasing wing structural weight. To this end, there is usually an optimum that lies along the constraint imposed as the field performance.

If, however, the penalties for having a large wing area are not severe enough, the optimization will exploit that fact and deem the larger wing area a valid tradeoff for increased cruise performance in the form of a reduced lift coefficient. If we examine the form of several wing weight equations with respect to the set of design variables used, we can gain greater insight into the differences in optimization results.

Nicolai Formula:

The wing weight as specified in *Fundamentals of Aircraft Design*[15] is given by,

$$W_{wing} = 0.00428\, K_s S_w^{.48} \frac{AR\, M_o^{.43}}{\{100(t/c)_{\max}\}^{.76}} \cdot \frac{(N W_{to})^{.84} \lambda^{.14}}{\cos^{1.54} \Lambda_{1/2}} \qquad (52)$$

Where M_o is the maximum Mach at sea level, N is the design load limit, and $\Lambda_{1/2}$ is the sweep at mid-chord.

Raymer Formula:

As found in *Aircraft Design: A Conceptual Approach*, the formulation of the wing weight is given by[13],

$$W_{wing} = 0.0051 K_s S_w^{0.649} S_{csw}^{0.1} \frac{AR^{0.5}}{(t/c)_{root}^{0.4}} \cdot \frac{(N W_{to})^{0.557} (1+\lambda)^{0.1}}{\cos \Lambda_{.25}} \tag{53}$$

where S_{csw} is the area of the flight control surfaces on the wing (S_{csw} =10% for this example) and $\Lambda_{.25}$ is the quarter-chord sweep.

McCullers[24] Formula:

This formulation is the most sophisticated, integrating estimated span loads to arrive at bending moment distributions and material factors. The wing weight is given by,

$$W_{wing} = \frac{W_{to} C W_1 + W_2 + W_3}{1 + W_1} \tag{54}$$

where

$$W_1 = C \cdot N \cdot b(1-0.4 f_c)(1-0.1 f_a) \tag{55}$$

$$W_2 = 0.68(1-0.17 f_c) S_{csw}^{0.34} W_{to}^{0.6} \tag{56}$$

$$W_3 = 0.35(1-0.30 f_c) S^{1.5} \tag{57}$$

and

$$C = 8.8 B_z \left[1 + \left(\frac{6.25}{b} \right)^{1/2} \right] \times 10^{-6} \tag{58}$$

We define f_c as a composite material factor (0-1) and f_a as an aeroelastic tailoring factor (0-1). B_z is the bending material factor computed from,

$$B_z = \frac{2V}{Ld} \tag{59}$$

where,

$$d = AR^{0.25}[1+(0.5f_a - 0.16)\sin^2 \Lambda_{L_{ave}} + 0.3C_Y(1-0.5f_a)\sin \Lambda_{L_{ave}}] \tag{60}$$

with $\Lambda_{L_{ave}}$ defined as the weighted average of the load sweep angle. The total load on the wing is given by,

$$L = \int_0^1 p(y)dy \tag{61}$$

with $p(y)$ as the pressure load, and the required volume of structure based on the stringer area, $A(y)$, as,

$$V = \int_0^1 A(y)dy \tag{62}$$

Figure 11. shows the effect of increasing wing area on both wing weight and total aircraft weight. Although the wing weights and corresponding takeoff weights are very close numerically (Note that the Nicolai and Raymer equations cross near the baseline wing area at 3500 ft^2) the gradients of the Raymer and McCullers equations are steeper, giving rise to a more severe penalty for a larger wing. We also notice that the Raymer and McCullers formulations give very similar gradients over the range of wing areas plotted. Compared to the Raymer equation, the actual takeoff weight values are roughly 4% less for McCullers over the range.

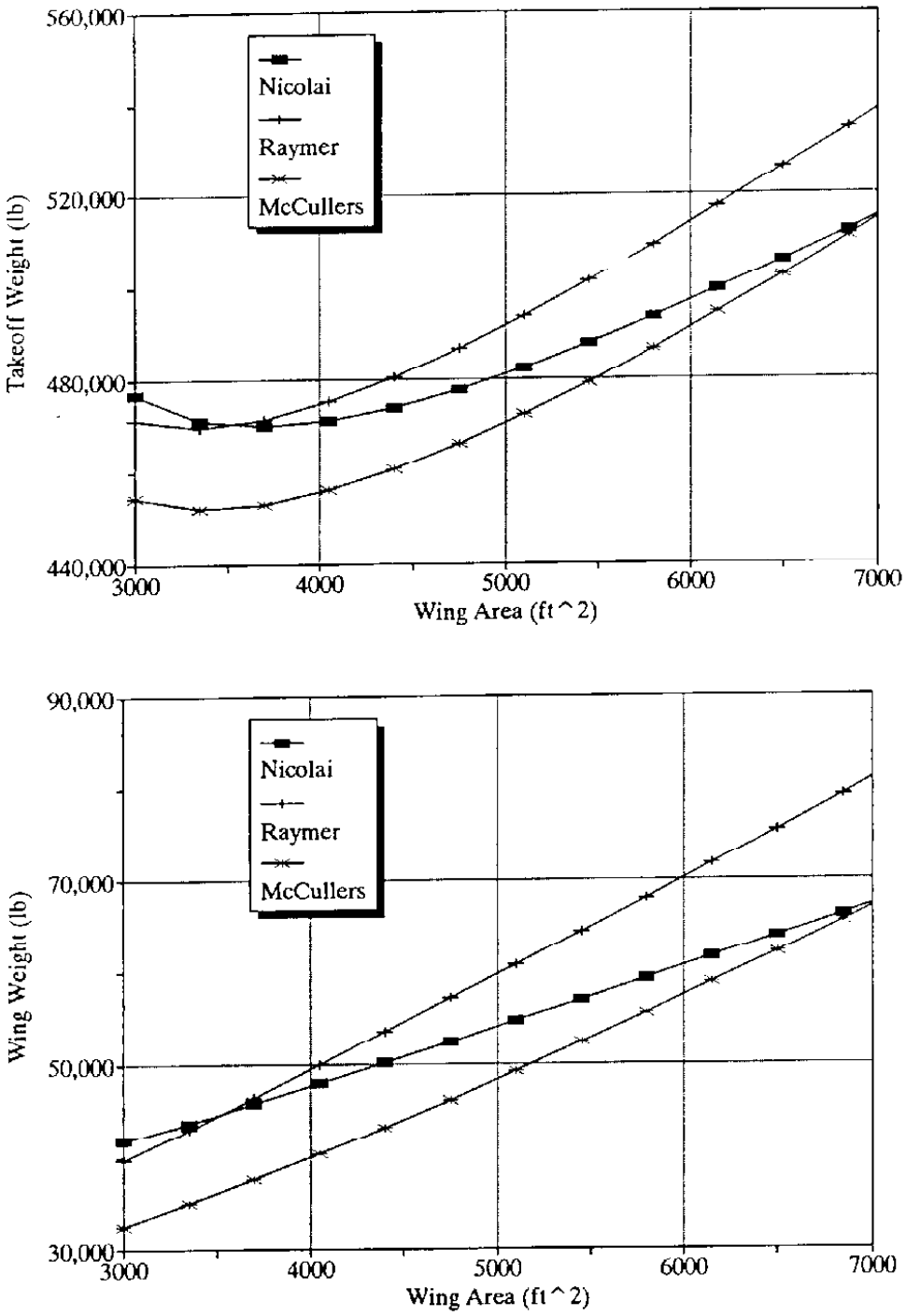

Figure 11. Effect of Wing Area on Several Wing Weight Models.

We now consider the aspect ratio effects. Figure 12. shows the variation of the wing weight and total takeoff weight for a range of aspect ratios. We see that the Nicolai formulation is much more sensitive to changes in aspect ratio than Raymer or McCullers. As in the wing area comparison, both Raymer and McCullers exhibit similar penalties over the range plotted. These two equations give results that are approximately 7% different in the overall aircraft weight. The relatively shallow gradient of the takeoff weight for the Raymer and McCullers equations is of interest from an optimization standpoint. It is this lack of aspect ratio penalty that leads the optimization to a large aspect ratio design as demonstrated in section 7.1.

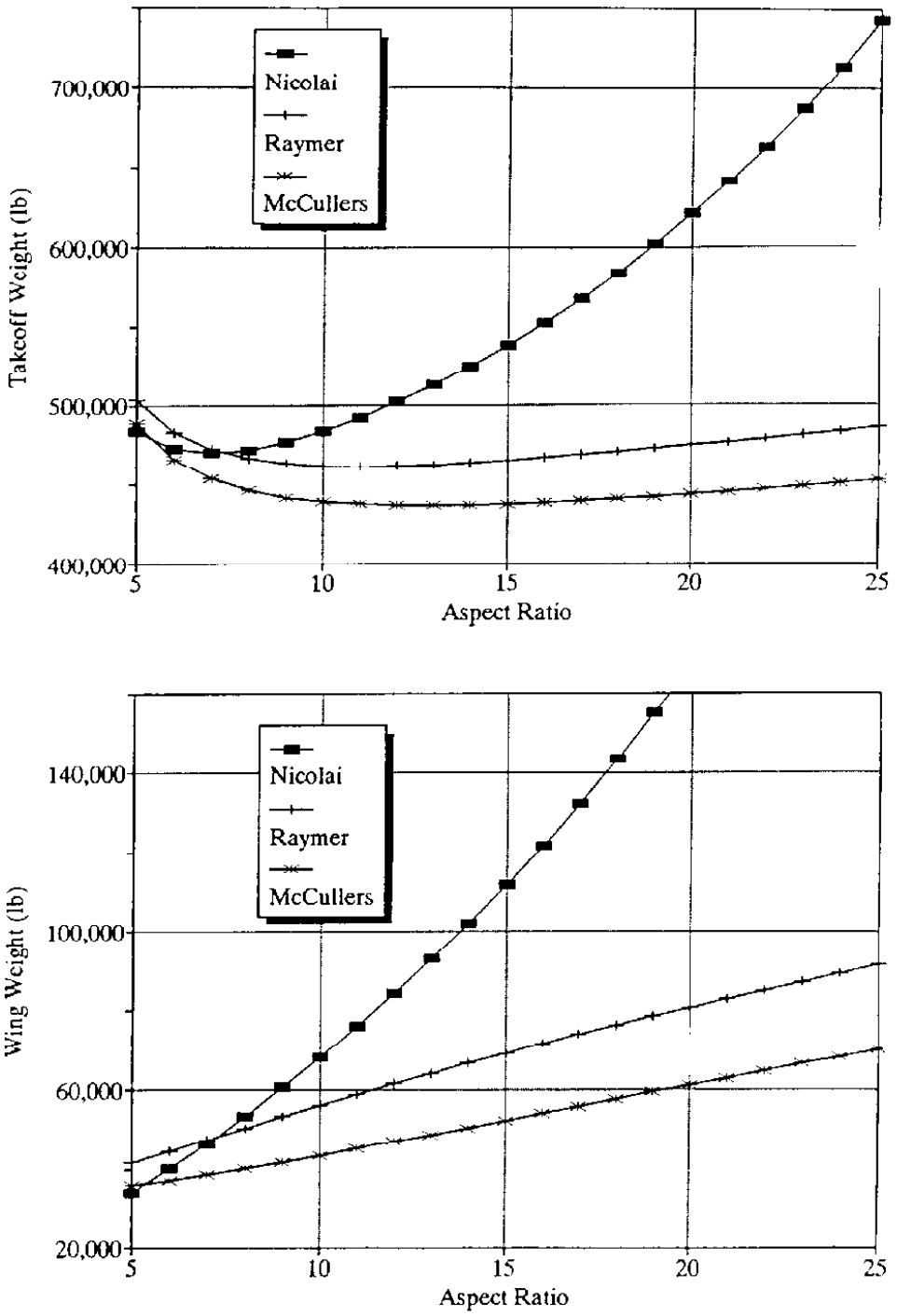

Figure 12. Effect of Aspect Ratio on Several Wing Weight Models.

8.2 Effect of Increased Complexity Wing Weight Models On Optimum

For the case at hand, the complete set of design variables is chosen. The objective function was the takeoff gross weight (W_{to}), and the mission was a 3000 nm cruise with a field performance constraint on the takeoff distance ($S_{to} < 5000$ ft).

Figure 13. illustrates the effect of using different wing structural weight models. By implementing a more sophisticated routine (McCullers) for calculating the wing weight, the results can be compared to the simpler analytic technology model. The first case is Raymer's wing weight equation, the second uses McCullers, and the third case uses Nicolai's wing weight equation.

We see from the figure that the McCullers equation results in the lowest weight solution, however the trends between all three models are very similar. The results using the McCullers formulation are very similar in overall trends to the Raymer results. The differences were approximately 9% over the entire range of Mach numbers. This similarity in trends is equivalent to the effects presented in the previous section.

Because the penalty on aspect ratio is so demanding, Nicolai's equation results in very high wing areas, which result in very short takeoff distances. Notice that the trend of wing area changes at every point where another design variable reaches an upper or lower bound. This occurs because the takeoff constraint is no longer active for these high wing areas.

If the optimum takeoff weight computed for the Raymer and Nicolai equations are compared, we see that the Raymer equation leads to a larger takeoff weight for each specified cruise Mach number. The interesting feature to note, however, is that the Raymer optima are steadily diverging from the Nicolai results. At the Mach = 0.6 optimum, the difference between the two results are 2.2%, whereas at M = 0.85, the difference is 4.8%. This gives rise to the question of the relative validity of the two

equations within the range of design variables used (Although each design is not absurd.) More to the point, however, is the question of the importance placed on the wing area and aspect ratio in each wing weight equation, and the direction that the optimization takes based on this information.

The important differences between Raymer's and Nicolai's equations are the powers to which the design variables are raised. In the case of the Nicolai equation, the aspect ratio power is one. Compared with the Raymer equation, where the wing weight is a function of the square root of the aspect ratio, the penalty for aspect ratio is much more severe in the Nicolai equation. This explains the behavior of the optimization to consistently arrive at a much smaller aspect ratio. In the cases where the specified cruise Mach was beyond 0.75, the aspect ratio was at the lower limit for each optimum. Using the Raymer formulation, however, gave a set of optimal aspect ratios that were larger, and more in accordance with advanced technology transport designs[25] This is a direct effect of the reduced penalty for aspect ratio in the Raymer equation. Interestingly, for both wing weight equations, the results followed the same trends, at least to the point where the aspect ratio for the Nicolai case was limited by the imposed lower bounds.

The optimum results for the wing area can also be explained through the examination of the penalty imposed for wing area in each formulation. For the Nicolai equation, the penalty is given by $S_w^{.48}$, compared to the Raymer penalty of $S_w^{.649}$. This again leads the optimization procedure to results that are less than intuitive for a range of specified Mach numbers. The penalty for wing area in the case of the Raymer equation is larger than that for the Nicolai equation. This leads to smaller optimum wing areas, and, in fact, leads to the sizing of the wing for the takeoff constraint (takeoff distance is at the limit imposed, or 'active'). On the other hand, the wing is sized for the cruise (in the form of a reduced C_L) when the wing weight penalty is not as harsh (Nicolai).

Finally, the tradeoff observed in the results illustrate how the optimization is fundamentally searching for an increase in span, either through the aspect ratio, or the wing area. At low cruise Mach numbers, the high aspect ratios illustrate a limitation structurally of the design. With the proper constraints imposed through structural limitations, both designs would be even more realistic as the slower cruise speeds would become less favorable.

The data presented supports no conclusions to the superiority of any one equation, and, if anything, it brings out the importance of using analytic technology models within a proper range of validity when coupled with numeric optimization techniques. Although each formulation leads to similar figures of merit, the aircraft designs that arise are drastically different simply as a result of the wing weight equation used.

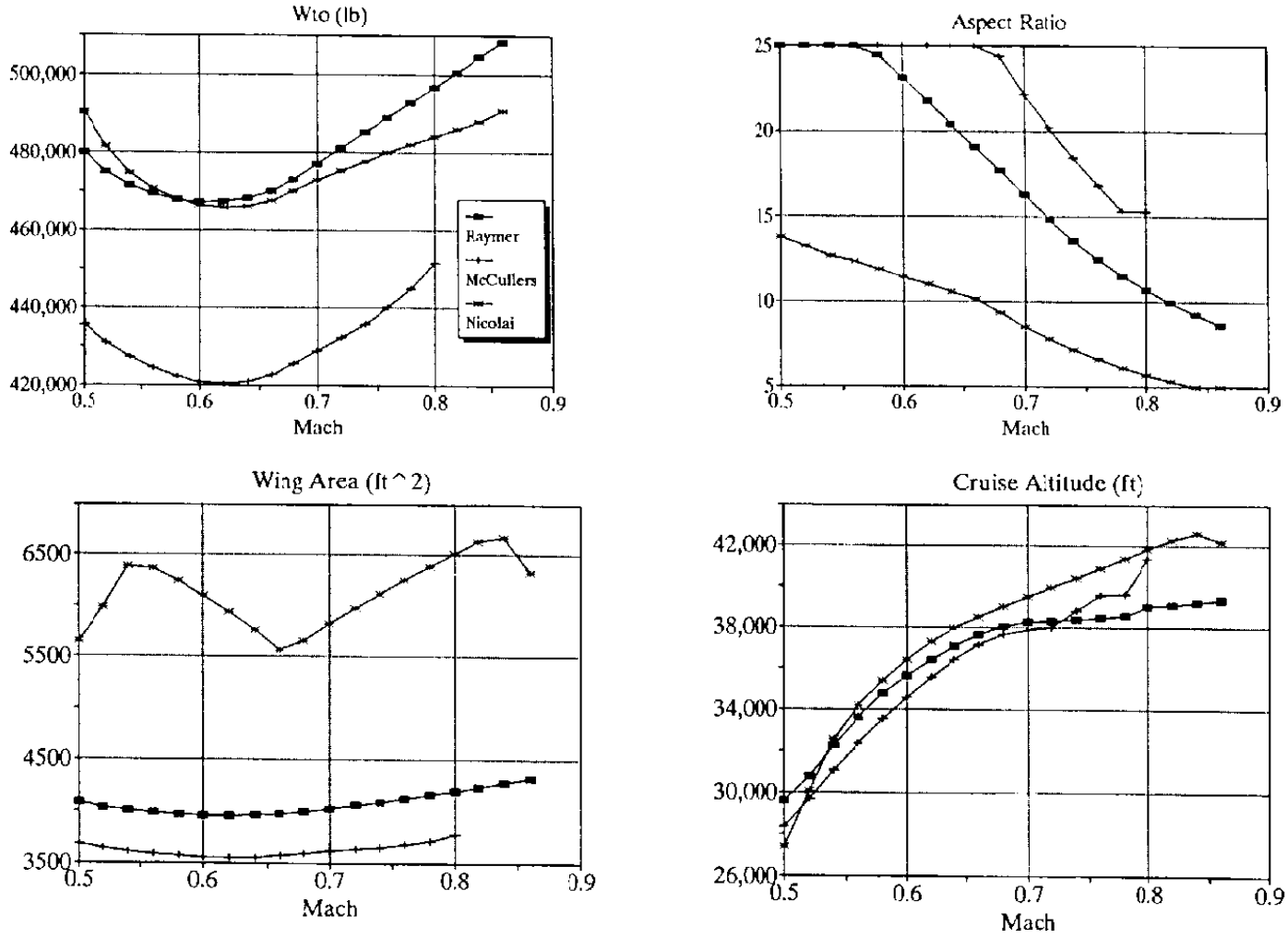

Figure 13. Effect of Increased Complexity (Wing Weight Models) on Optimum.

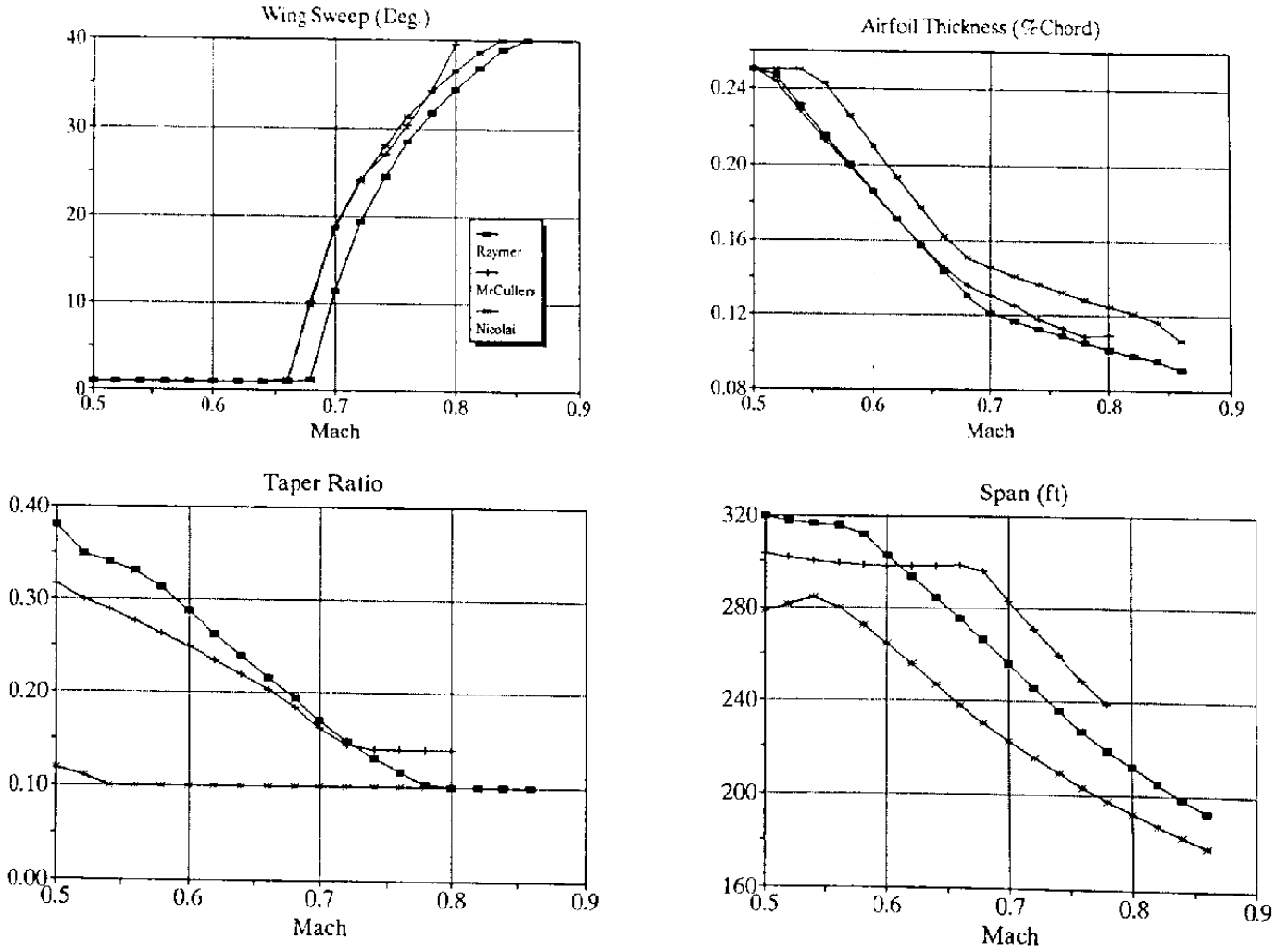

Figure 13. (Continued) Effect of Increased Complexity on Optimum.

9. Optimization Demands on Technology Integration

9.1 Smoothness

Even though the functions used for the technologies are smooth and analytic, the methods by which the derivatives for the GSE system are calculated (i.e. finite difference) must produce very accurate results. Convergence to very tight criteria is important if the system is going to be 'mass optimized', that is, to produce a set of optimal solutions over a range of a certain design variable. If each solution is not optimized to within a very strict tolerance, the plots of each optimum design variable will not exhibit a smooth pattern.

9.2 Initial Point Selection for Range of Optimum

In any optimization procedure, the selection of the initial point is crucial. Two basic methods were used to implement initial point for the optimizer in this research. One is to specify the initial point as some fixed point that is used for all Mach numbers. The observation with this method is that the initial point must be specified such that the system can be converged to a solution over the entire range of Mach numbers. That is, a suitable initial point must be selected such that the a takeoff weight can be obtained. As described previously, the method used is a fixed point iteration sizing scheme. A 'middle-of-the-road' value must be selected for the initial point when using this method.

The second method of implementing initial point is to use the optimal solution of the previous Mach number as the initial point into the new Mach number. This method also has the problem as described above, but on a smaller scale. The optimal solution only needs to be convergent at the next Mach number. Theoretically, this is not difficult to insure, however, it has not been proven if this can be guaranteed. Another issue with

using this type of initial point selection is that the design could wander into an another valley of optimal solutions. This illustrates the presence of local optima.

An example of the differences that can arise as a result of initial point implementation is shown in Figure 14. This figure employs the McCullers wing weight equation, and an initial point that is convergent for a low Mach number. This means that the design variables were such that they were close to the solution for a low specified Mach number. Case 1. specifies the initial point of the current Mach number as the optimal solution of the previous Mach number. Case 2. specifies the same initial point over the entire Mach range.

We observe from the figure that Case 1. leads the optimization into a range of local minima over the Mach range of 0.70-0.74. The optimization recovers at M=0.76 as it locates the proper solution. By comparing the plots of wing sweep and airfoil thickness, we can gain insight into the path of the optimization. The most noticeable feature is that the optimization chose to reduce the transonic drag rise by continuing the reduction of thickness while maintaining a zero sweep configuration. The sweep was not used to alleviate the transonic drag rise until M=0.76, as compared to Case 2., where the sweep was employed at M=0.70. The interesting item to note from this figure is the differences in trade-offs the optimization employed for a given initial point method. By keeping the sweep low, the optimization process lead to a design with a structurally light, yet aerodynamically inferior wing.

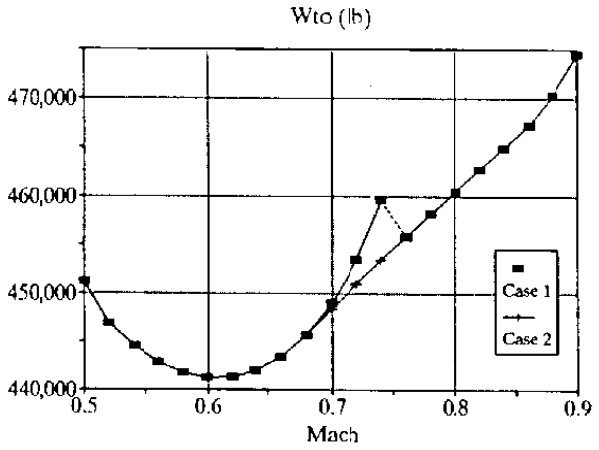

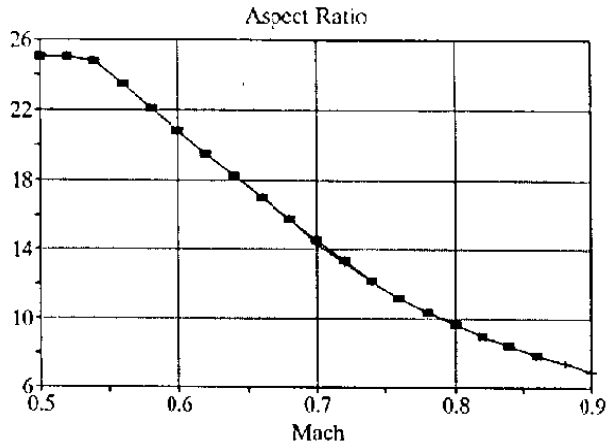

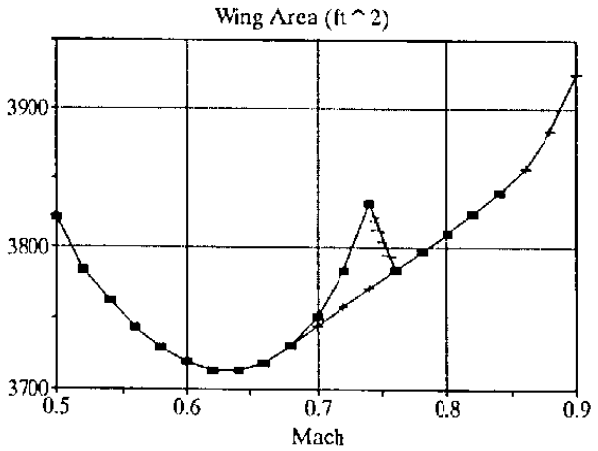

Case 1. Begin initial point for optimization using the optimal solution from the previous Mach number.

Case 2. Define initial point for optimization same for all Mach numbers.

Figure 14. Effect of Initial Point Selection.

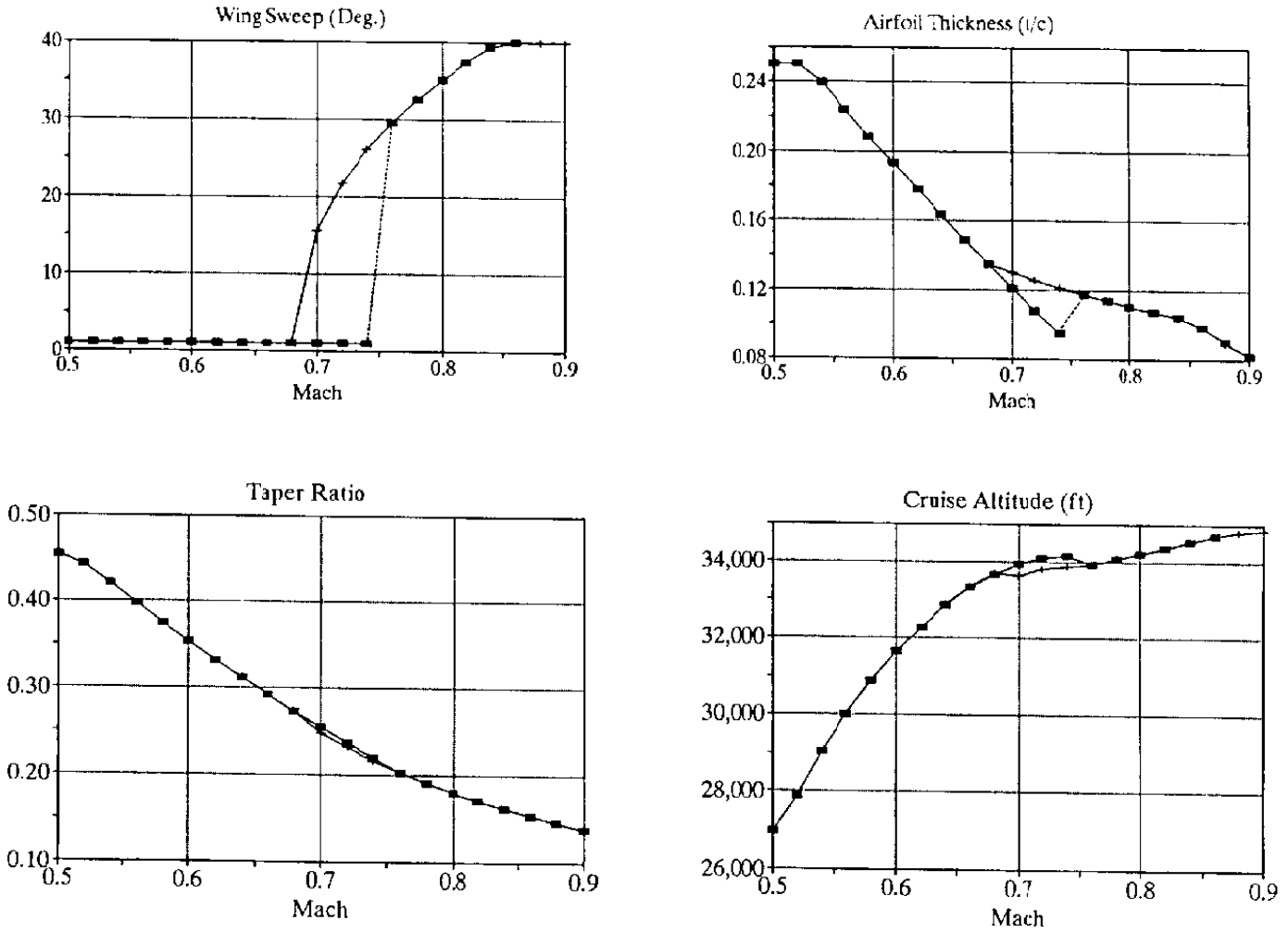

Figure 14. (Continued) Effect of Initial Point Selection.

10. Effect of Objective Function

The importance of the figure of merit within an optimization problem can be examined by using the methods described in previous sections and taking advantage of the rapid computational time afforded by the analytic expressions for the various technology models. The results presented thus far have utilized the takeoff gross weight solely as the objective function. To gain a greater understanding of the designs that evolve using this figure of merit, it is of interest to consider various alternate objective functions, such as a specific component weight, or a cruise performance parameter. One can also parametrically optimize, as done with the cruise Mach number, using a range of objective functions. The results show the evolution of the design from, for example, a performance optimized solution, to a structurally optimized solution.

10.1 Parametric Objective Function Formulation

As indicated above, we can define a range of objective functions that can be used in multiple optimization cases to illustrate the evolution of a design from one figure of merit to another. This can be accomplished by defining the objective function in the following manner,

$$F = K_o F_{obj1} + (1 - K_o) F_{obj2} \tag{63}$$

where K_o is varied from 0 to 1. When K_o = 1, the objective function is given entirely by the first objective, F_{obj1}, and when K_o = 0, the objective function is entirely F_{obj2}. When K_o is between 1 and 0, then the overall objective function is given by a combination of the two.

10.2 Solutions for Minimizing Fuel Weight and Wing Weight

We select the cruise fuel weight, given by eqn (16), and the wing structural weight, eqn (15), as the two figures of merit to minimize. The formulation for the objective function for this case is then given by,

$$F = K_o W_{Wing} + (1 - K_o) W_{Fuel} \tag{64}$$

As defined earlier, the takeoff constraint of 5000 ft is imposed along with the section lift coefficient limit. By prescribing the figure of merit in the fashion shown above, the design can be selectively optimized to minimize the wing weight when K_o is 1, the fuel weight when K_o is 0, or any combination of the two when K_o is between 1 and 0. The resulting solutions reflect the shift from a fuel minimized, cruise efficient design, to a structurally efficient design as K_o is increased from 0 to 1. This tradeoff illustrates the importance of proper objective function selection and the relative influence of each component when the total aircraft weight is used as a figure of merit.

Figures 15.1-15.3 show the results of using eqn (64) as the objective function in the optimization routine. Figure 15.1 shows that there is a penalty in overall gross weight when either the fuel or wing weight is minimized alone. The minimum gross weight occurs for a value of K_o = 0.2. We see from Figure 15.2 that for the minimum fuel weight solution the aspect ratio is at the upper limit of 25, and the wing area is slightly less than 4600 ft^2. Notice from Figure 15.3 that the specific range is at its largest value. As the influence of the wing structural weight is increased in the objective function, the design shifts to a low aspect ratio, low specific range design. We see the optimum cruise Mach number changes from 0.72 (K_o = 0) to just under 0.60 (K_o = 1). The wing area decreases as K_o moves from 0.0 to 0.2, then increases to a maximum of just over 5000 ft^2 at K_o = 1. As seen in the previous sections, the decreasing aspect ratio is the result of

the penalty in the wing weight equation arising from the aspect ratio. For increasing values of K_o, the influence of fuel weight in the objective function is reduced, and the resulting designs show a reduction in the specific range as well as the cruise Mach number.

The relative weightings of both the wing weight and the fuel weight in the total takeoff weight formulation are illustrated in the plot of the takeoff weight. We see that for K_o = 0.2, W_{to} is a minimum. This shows that if W_{to} were used as the objective function, as done in the previous sections, the result would be 20% influence of wing structural weight and 80% fuel weight.

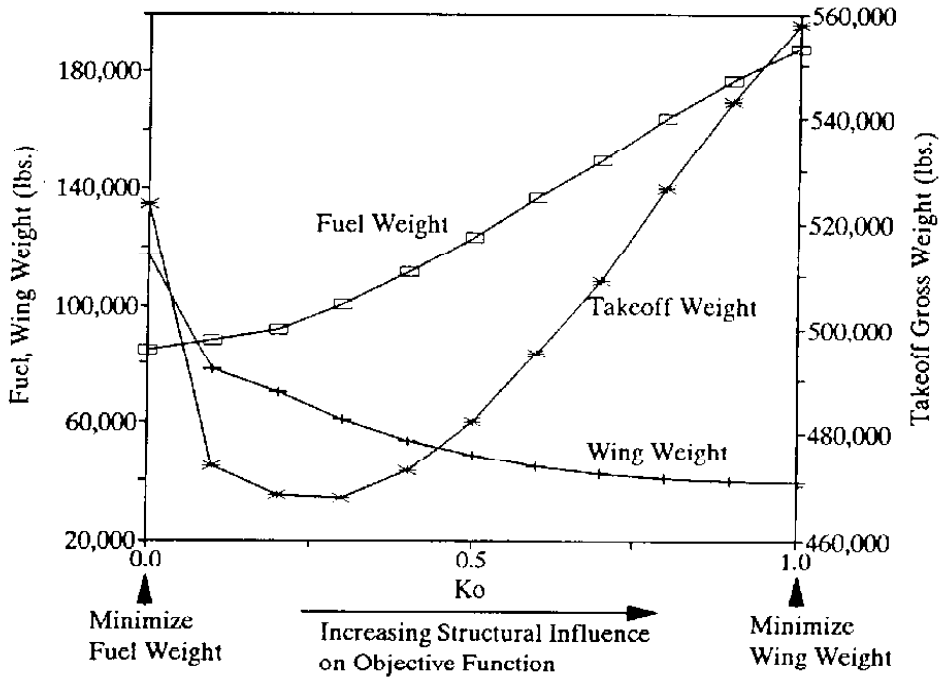

Figure 15.1 Minimum Fuel / Wing Weight Solutions.

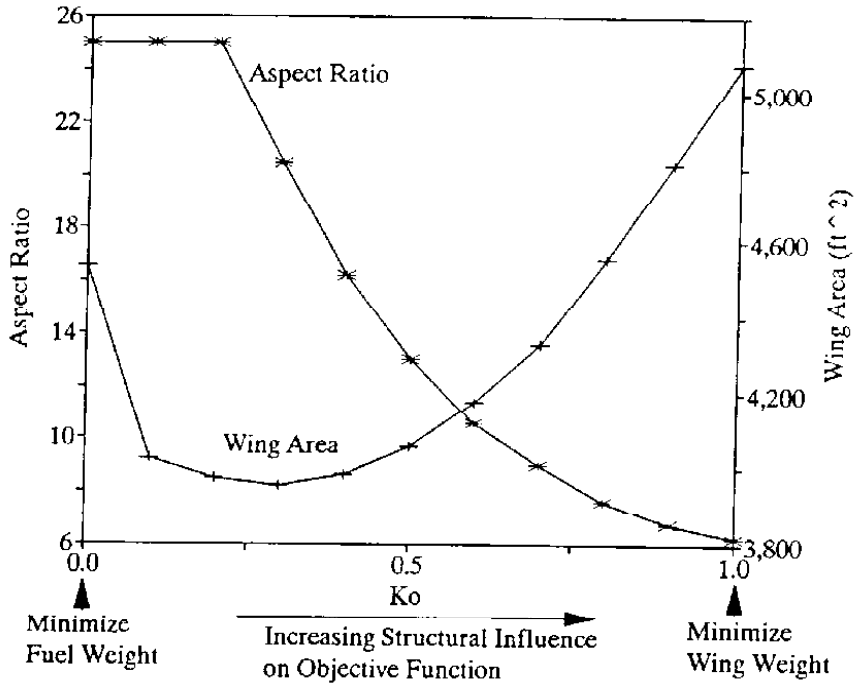

Figure 15.2 Minimum Fuel / Wing Weight Solutions.

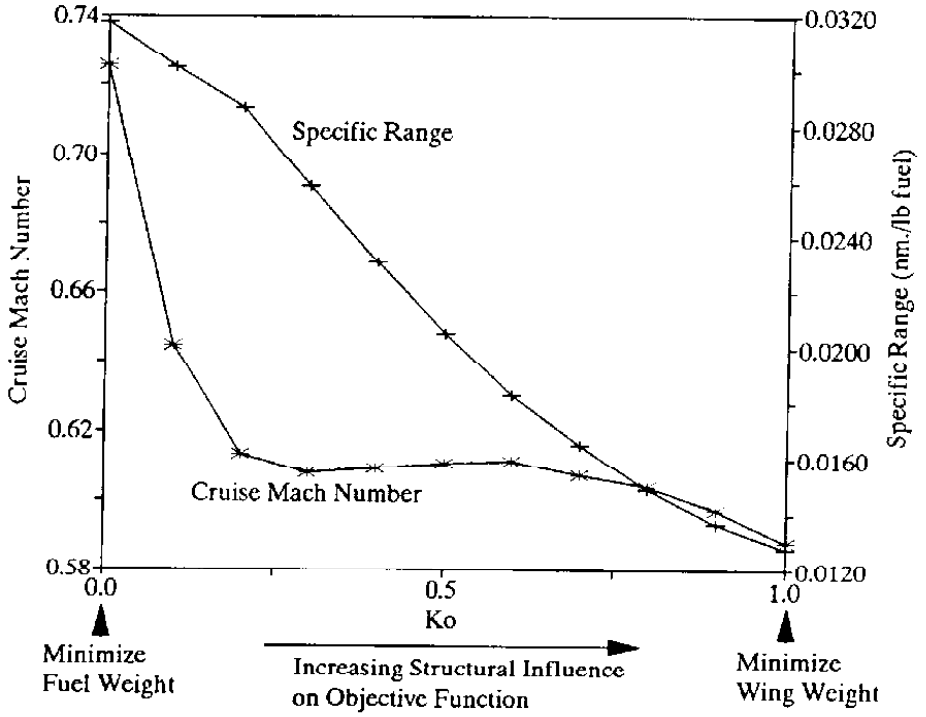

Figure 15.3 Minimum Fuel / Wing Weight Solutions.

10.3 Solutions for Maximizing the Range Parameter and Minimizing the Wing Weight

The cruise efficiency of the aircraft can be embodied in the range parameter, given by

$$R_p = \frac{M\left\{\frac{L}{D}\right\}}{sfc} \tag{65}$$

This expression can then be used in the formulation of the multiobjective function as follows,

$$F = K_o W_{Wing} + (1 - K_o)(-R_p) \tag{66}$$

where in order to maximize the range parameter, denoted here as R_p, we minimize the negative of the function. Again, the takeoff and the section lift coefficient constraints are imposed at the same values used for the case described in section 10.2.

Figures 16.1-16.4 show the results of this objective function and the effect of increasing the structural influence as K_o is varied from 0 to 1. Compared to the minimum fuel solution, the takeoff weight found in Figure 16.1 is dramatically increased when the range parameter is the sole objective function (K_o = 0). The weights decrease very quickly for increasing influence of structural weight on the figure of merit, however. As opposed to minimizing the fuel, maximizing the range parameter results in the wing area and the aspect ratio being driven to their respective upper bound, as found in Figure 16.2 With a strong influence of cruise efficiency on the design, the cruise Mach number, shown in Figure 16.3, is very high compared to a structurally efficient design. With the high Mach numbers come the large wing sweep angles. The wing sweep is sharply reduced as the Mach number begins to decline. Interestingly, the Mach number and wing sweep initially begin to increase for values of K_o from 0.0 to 0.06 as the wing area begins to decrease and the taper ratio is held at its lower limit. We also see

that the takeoff weight is minimum at K_o = 0.4, compared to the minimum fuel solution where K_o was 0.2.

The fuel weight is not at a minimum for the maximum range parameter. The plot of the specific range, Figure 16.4, which includes the effect of takeoff weight, shows a maximum where the fuel weight is minimum, K_o = 0.2. The specific range is very similar to the range parameter,

$$S_R = \frac{V_{Cruise}\left\{\frac{L}{D}\right\}}{sfc \cdot W_{to}} \tag{67}$$

however, the specific range considers the effect of altitude, as well as the takeoff weight.

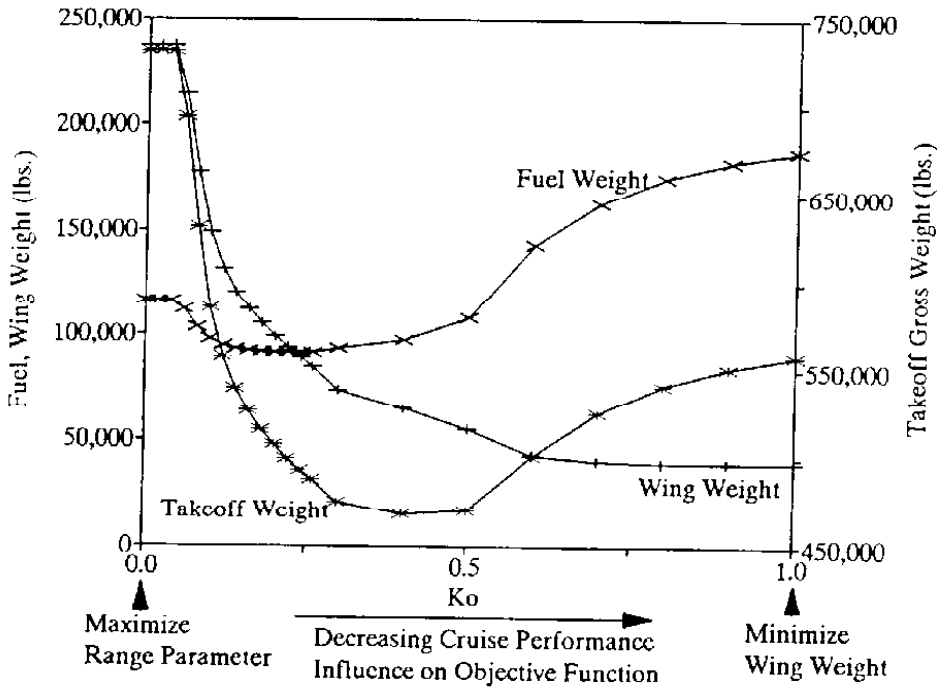

Figure 16.1 Maximum Range Parameter / Minimum Wing Weight Solutions.

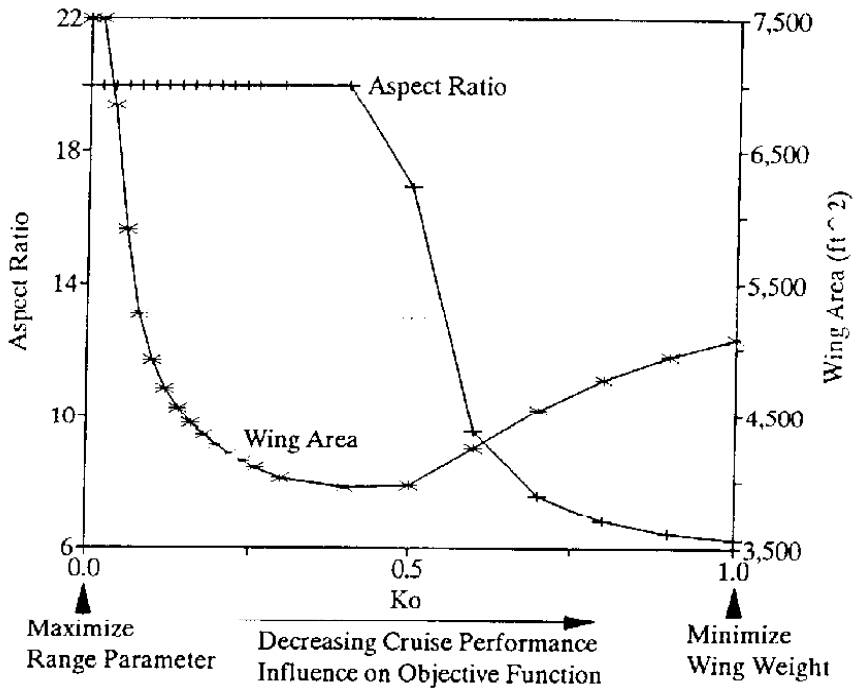

Figure 16.2 Maximum Range Parameter / Minimum Wing Weight Solutions.

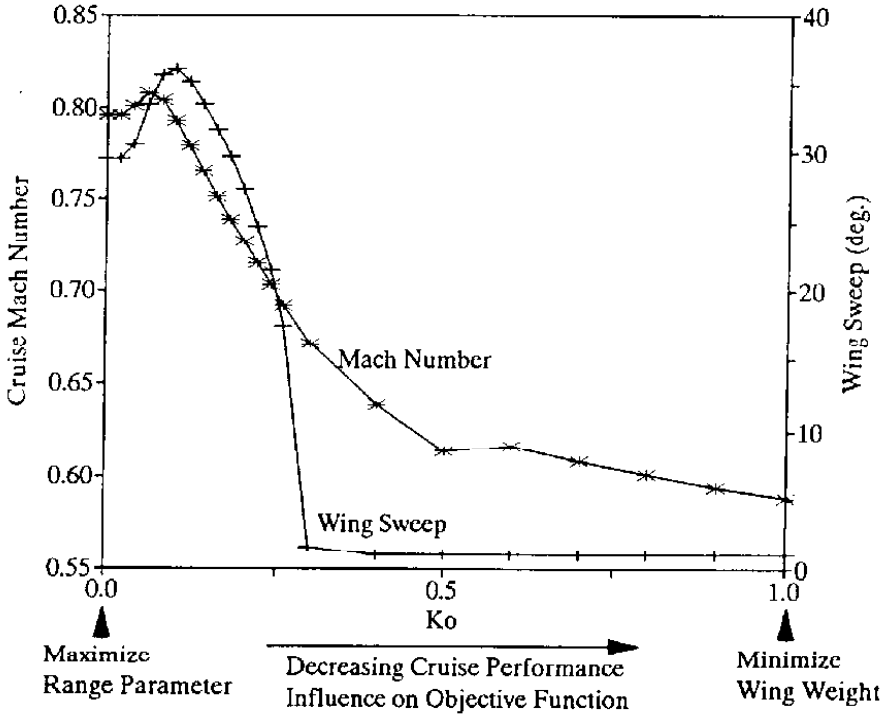

Figure 16.3 Maximum Range Parameter / Minimum Wing Weight Solutions.

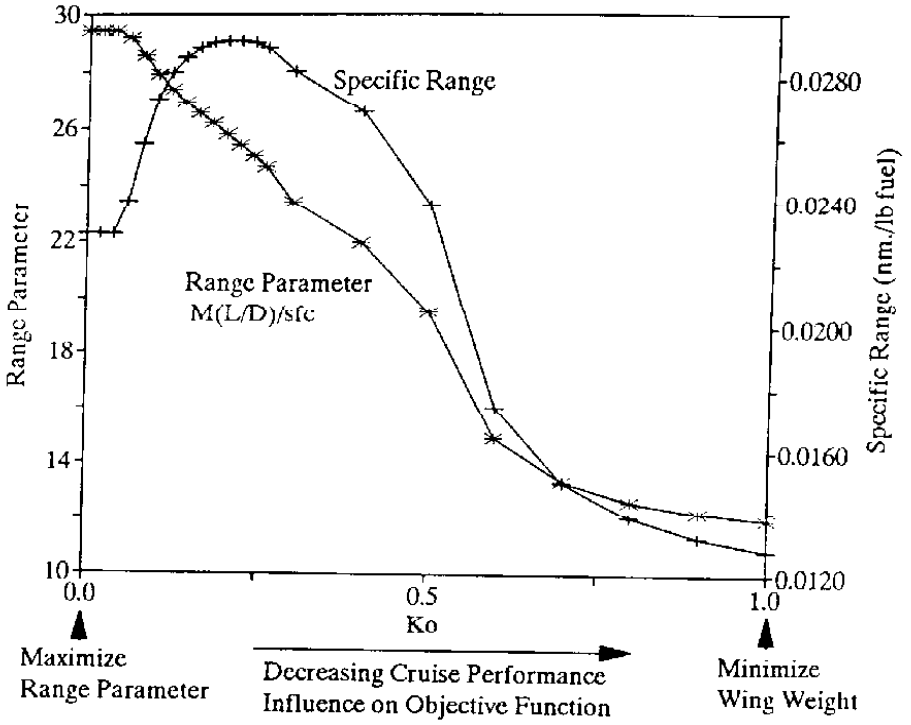

Figure 16.4 Maximum Range Parameter / Minimum Wing Weight Solutions.

10.4 Maximizing Productivity

We can define the specific productivity of a given aircraft by the following,

$$\frac{W_{Payload} \cdot V_{Cruise}}{W_{Fuel}} \tag{68}$$

It is economically advantageous to maximize the productivity of a certain design. Because the payload weight is fixed for the given analysis, we see that to maximize the productivity is to minimize the fuel/velocity ratio. Therefore, with this objective function, we expect to see increased cruise Mach numbers, while maintaining fuel efficient planforms, i.e. high aspect ratio.

Table 5. shows the results of maximizing the productivity. As expected, the cruise Mach number is much higher than any of the minimum weights solutions. The penalty

for the productivity, however, is the large takeoff gross weight, 21% larger than the minimum W_{to} solution. The aspect ratio of 20.1 is less than the prescribed upper bound. This aspect ratio is also less than that for the minimum W_{to} solution.

Table 5. Results for Maximizing Productivity.

Design Variables	
Aspect Ratio	20.1
Wing Area	5,424 ft^2
Cruise Altitude	46.621 ft
Cruise Mach Number	.846
Wing Sweep	40.0 deg.
t/c	0.07
Taper Ratio	.14
Weights	
Fuel	91,762 lb
Wing	164,398 lb
Engine	30,000 lb
Fixed	149,370 lb
Climb Fuel	11,949 lb
Cargo	150,000 lb
Takeoff Gross Weight	597,481 lb

10.5 Comparison of Results from Various Objective Functions

Table 6. shows the results for the different objective functions described above. We can see the differences in the design variables reflect either a highly cruise efficient design, or a structurally efficient design, depending on the figure of merit used. Notice that for the minimum wing weight solution, the fuel weight is more than double that of the minimum fuel solution. This shows the large aerodynamic penalty incurred for the lower aspect ratio designs. Also, the cruise altitude is much lower for the minimum wing

weight solution than the other results. This is due to the low aspect ratio / high wing area design. Finally, as a result of the weight penalty for thin airfoils, we see the airfoil thickness is much larger for the minimum wing weight solution than for the other designs.

Table 6. Comparison of Results from Various Objective Functions

	Minimum Gross Weight	Minimum Fuel Weight	Minimum Wing Weight	Maximum Productivity	Max.Range Parameter
Design Variables					
Aspect Ratio	22.6	25.0	6.2	20.1	20.0
Wing Area (ft^2)	3,958	4,539	5,072	5,424	7,500
Altitude (ft)	35,983	44,107	22,964	46,621	40,000
Mach Number	0.607	0.725	0.588	.846	0.796
Wing Sweep (deg.)	1.0	26.9	1.0	40.0	29.5
t/c	0.18	0.09	0.24	0.07	0.05
Taper Ratio	0.28	0.28	0.10	0.14	0.10
Weights					
Fuel (lb)	96,614	84,649	187,779	91,762	116,860
Wing (lb)	64,512	117,630	39,518	164,398	237,570
Engine (lb)	30,000	30,000	30,000	30,000	30,000
Fixed (lb)	116,824	130,917	139,485	149,370	183,024
Climb Fuel (lb)	9,345	10,473	11,158	11,949	14,641
Cargo (lb)	150,000	150,000	150,000	150,000	150,000
Gross Weight (lb)	467,298	523,671	557,942	597,481	732,097

Figure 17. shows the breakdown of component weights for several of the objective functions described above. We see that most of the additional weight for the maximum productivity solution comes from the wing structural weight. Because each design shown in Figure 17. is a high aspect ratio solution, the increased structural weight of the maximum productivity solution is due to the additional wing sweep necessary for the

transonic cruise Mach number. Also, the minimum gross weight solution leads to the lowest wing structural weight. Again, this is in direct relation to the cruise flight conditions because the minimum gross weight solution has the lowest cruise Mach number.

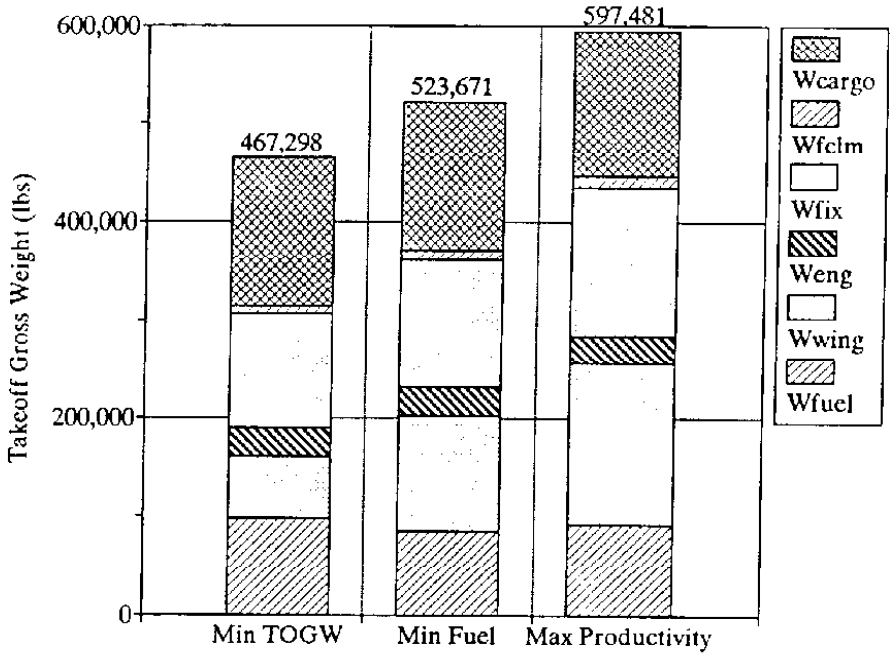

Figure 17. Component Weight Breakdown for Several Objective Functions.

11. REMARKS AND CONCLUSIONS

The approach to multidisciplinary optimization proposed here for use at the conceptual/preliminary design level provides the designer with a wealth of information with a minimal investment in time. The following is a summary of the lessons learned and resulting recommendations for use of this approach.

Optimization :

- Smooth analytic models work best with optimization.
- Precise gradient information (numerically accurate tolerances) required.
- Sensitivity to model accuracy: optimization exploits the peculiarities of any model.

Problem formulation:

- Independent variables are sometimes hard to identify. Analytic models provide a fast way to examine the formulation and results from the problem formulation. TOGW was made a separate discipline as a result of the problem analysis at this stage.

Value of Parametrics Optimized Solutions:

- Integrity of Results: without parametric studies, erroneous optimization solutions (local minima, uncertainty due to inaccurate gradients) are very hard to identify. This has been the reason that optimization hasn't been used by designers in the past.

Using analytic models:

- The benefits of the analytic modelling is the multitudes of optimized results that can be created cheaply. At present, for a range of a certain parameter, a set of twenty

optimized solutions can be run in approximately 4.6 cpu minutes on the IBM 3090 system.

- It's easy to identify explicitly the role of individual design variables and constraints.
- Regarding the wing weight equation, by making the jump from a simple one line equation to an entire set of routines that integrate a given pressure loading and solves for bending moment factors, the concept of *Variable Complexity* was demonstrated.

Global Sensitivity equations.

- Gradient information is controlled by the user, and provided to the optimizer.
- Explicit sensitivities are available for examination at each step.

Furthermore, the GSE method is desirable because it gives the same results as a finite difference based derivative scheme for less computations based on several key problem dependent issues:

i.) The number of subsystems

ii.) The number of design variables

iii.)The accuracy to which the entire system is converged

iv.)The complexity of the subsystems

v.) The size, density, and method of inverting the GSE matrix

vi.)The finite difference method used (central vs. forward)

The system can be setup to replace analytic models with more exact analytic or numerical models. This was done in the case of the wing weight model. It is recommend

that this approach always be used with analytic models before using more exact numerical analysis.

- Information flow is defined exactly. Valuable insights into both the problem formulation and the behavior of the solution are available in days rather than weeks using this approach.

- This approach can provide a starting point for the optimization using more detailed calculation procedures.

The approach described here provides a means of bridging the gap between formalized optimization methodology and aircraft sizing programs which are currently in use. In conclusion, this new method is a simple way of gaining greater insight into the problem of aircraft design and initial sizing.

REFERENCES

1. Vanderplaats, G., "Automated Optimization Techniques for Aircraft Synthesis," AIAA Paper 76-909, September 1976.

2. S.G. Wampler, A. Myklebust, S. Jayaram, and P. Gelhausen, "Improving Aircraft Conceptual Design - A PHIGS Interactive Graphics Interface for ACSYNT," AIAA Paper No. 88-4481, September 1988.

3. Sobieszczanski-Sobieski, J., "Multidisciplinary Optimization for Engineering Systems: Achievements and Potential", Proceedings of an International Seminar, *Optimization: Methods and Applications, Possibilities and Limitations*, Lecture Notes in Engineering 47, Bergmann, H.W., ed., Spring-Verlag, Berlin, 1989.

4. Sobieszczanski-Sobieski, J., "On the Sensitivity of Complex, Internally Coupled Systems," AIAA Paper 88-2378, April 1988.

5. Levine, M., Ide, H., and Hollowell, S., "Multidisciplinary Hypersonic Configuration Optimization," Proceedings of the Third Air Force/NASA Symposium on Recent Advances in Multidisciplinary Analysis and Optimization, San Francisco, 1990.

6. Logan, T. R., "Strategy for Multilevel Optimization of Aircraft," *Journal of Aircraft*, Vol. 27, No. 12, December 1990, pp. 1068-1072.

7. Hajela, P., Bloebaum, C., and Sobieszczanski-Sobieski, J., "Application of Global Sensitivity Equations in Multidisciplinary Aircraft Synthesis," AIAA Paper 89-2135, July 1989.

8. Dollyhigh, S.M., and Sobieszczanski-Sobieski, J., "Recent Experience With Multidisciplinary Anlysis and Optimization in Advanced Aircraft Design," Proceedings of the Third Air Force/NASA Symposium on Recent Advances in Multidisciplinary Analyis and Optimization, San Francisco, 1990.

9. Mason, W.H., "Analytic Models for Technology Integration in Aircraft Design," AIAA Paper 90-3262, September 1990.

10. Unger, E.R., Hutchison, M.G., Haftka, R.T., and Grossman, B., "Variable Complexity Interdisciplinary Design of a Transport Wing," Paper Presented to the Pan American Congress of Applied Mathematics, Valparaiso, Chile, January 1991.

11. Haftka, R.T., "Combining Global and Local Approximations," Technical Note, *AIAA Journal*, Vol. 29, No. 9, September, 1991, pp. 1523-1525.

12. Hildebrand, F. B., *Advanced Calculus for Applications*, Prentice-Hall, New Jersey, 1962.

13. Raymer, D., *Aircraft Design: A Conceptual Approach*, American Institute of Aeronautics and Astronautics Inc, 1989.

14. Torenbeek, E., *Synthesis of Subsonic Airplane Design*, Delft University Press, 1988.

15. Nicolai, L. M., *Fundamentals of Aircraft Design*, Mets, Inc., 1975.

16. Hilton, W.F., *High Speed Aerodynamics*, Longmans, Green & Co., London, 1952.

17. Inger, G., "Application of Oswaititsch's Theorem to Supercritical Airfoil Drag Calculation," AIAA Paper 91-3210, September, 1991.

18. Krekel, A.R., and Salzman, A.,"Takeoff Performance of Jet-Propelled Conventional and Vectored-Thrust STOL Aircraft", *Journal of Aircraft*, Vol. 5, No. 5, Sept-Oct, 1968, pp. 429-433.

19. Roskam J., *Airplane Design - Pts I-VII*, Roskam Aviation and Engineering Corporation, 1988.

20. Jensen, S.C., Rettie, I.H., and Barber, E.A., "Role of Figures of Merit in Design Optimization and Technology Assesment", *Journal of Aircraft*, Vol. 18, No. 2, Feb, 1981, pp. 76-81.

21. *Janes All the Worlds Aircraft 1988-1989*, Jane's Defence Data, Jane's Information Group Limited, Alexandria, VA, 1988.

22. Schittkowski, K., "NLPQL: A FORTRAN Subroutine Solving Constrained Nonlinear Programming Problems," Annals of Operations Research, pp 485-500, 1985- 1986.

23. Kress, R.W., "Variable Sweep Wing Design", AIAA Paper 80-3042, March, 1980.

24. McCullers, L. A. "Aircraft Configuration Optimization Including Optimized Flight Profiles", NASA CP-2327, *Proceedings of Symposium on Recent Experiences in Multidisciplinary Analysis and Optimization*, J. Sobieski, compiler, April 1984, pp. 395-412.

25. Lowery, R., "Evolution of Transport Wings From C130, C-141, C-5, to C-XX", AIAA Paper 80-3038, 1980.

APPENDIX. CODE DESCRIPTION

The computer code was designed in an organized fashion that followed the contributing analysis thinking. An automated 'black box' procedure was established that made computing the local derivatives and the global sensitivity matrix straightforward. By setting up the problem in a black box fashion, every discipline was an independent routine that modeled, what might be on a larger scale, an entirely separate analysis program. The flow of data between these routines was controlled such that the inputs of any one discipline were strictly a function of the outputs of the other disciplines. Communication between each discipline was done entirely through these **Y** vectors.

The code has the ability to run many various cases ranging from a simple one-pass converged weight solution, to an entire range of optimal solutions for a specified set of Mach numbers. The subroutine FUNCHEK is controlled by the integer ID1 and can perform many intermediate calculations at various steps in the optimization process. Parametrics can be run on any two design variables for contour plots, the objective function can be monitored as any one, or all of the design variables are run within a specified range, as well as cruise specific information in the form of specific range calculations. (Subroutine SRANGE)

The optimization flags supported include all the settings for NLPQLD (IPRINT) as well as derivative specific flags for monitoring the gradients of the constraints and objective functions at each iteration. Also supported is a flag, IHIST, for convergence histories for all the design variables as well as the objective function and constraints.

There are 6 source files that contain all the code and an input file.

NQCON.f — This is the controlling subroutine, all initialization and optimization calls are done here.

BBOX1.f	All of the subsystem coupling routines are found in this routine. GSE matrix and local derivatives. The global sensitivities are also computed in this routine.
BBOX2.f	This file contains all the technology model subroutines including the routine for takeoff, landing, and the standard atmosphere. Routines for converging the aircraft to a certain mission weight using fixed point iteration is also included in this file.
NQP.f	This file contains all of the nonlinear sequential quadratic programming routines except for the actual quadratic programming algorithm.
QLD.f	K. Shittkowski's quadratic programming algorithm
LINSOL.f	Linear system solver used to solve the GSE matrix.
BBOX.inp	Input file

INPUT DESCRIPTION FOR OPTIMIZATION DESIGN CODE

Input for the code is supplied in the file **BOX.inp**. The inputs found in this file are described in this section.

IOPTIM

IOPTIM = 0 NO OPTIMIZATION
= 1 OPTIMIZE SPECIFIED CONFIGURATION

ID1

CONTROLS SUBROUTINE FUNCHEK

ID1 = 1 ONE PASS THROUGH (CONVERGE A/C AND OBTAIN GLOBAL DERIVATIVES
= 2 CONTOUR PLOT DATA (SPECIFY 2 DESIGN VARIABLES)
= 3 L/D VS. CL DATA
= 4 PARAMETRICS OF EACH DESIGN VARIABLE
= 5 ZERO LIFT DRAG BREAKDOWN
= 6 ADDITIONAL RESULTS OF OPTIMA FOR RANGE OF M
= 7 SIMILAR TO ID1=4 EXCEPT NO DERIVS

ISR

USED FOR SPECIFIC RANGE CALCULATIONS

ISR = 0 NO SR OUTPUT
= 1 SPECIFIC RANGE OUTPUT

IPRT

USED FOR BLACK BOX DERIVATIVE OUTPUT

IPRT = 0 NO OUTPUT
= 1 OUTPUT

IDERIV

USED FOR OPTIMIZATION GRADIENT DERIVATIVE METHOD

IDERIV = 0 FINITE DIFFERENCE DERIVATIVES
= 1 GSE DERIVATIVES

IHIST

USED FOR CONVERGENCE HISTORY OF DV'S AND OBJ

IHIST = 0 OFF
= 1 ON

IWTEQN
USED FOR WING WEIGHT EQUATION
IWTEQN = 1 NICOLAI
= 2 RAYMER
= 3 MCCULLERS

Furthermore, inputs are required to describe the range of Mach numbers and the initial point to be used in the optimization procedure. These are defined as follows:

NJ
THE NUMBER OF MACH NUMBERS TO BE OPTIMIZED

MBEGIN
STARTING MACH NUMBER FOR MACH RANGE

MSTEP
MACH STEP USED IN RANGE

AR
ASPECT RATIO

SW
WING AREA

H
CRUISE ALTITUDE

SWEEP
WING SWEEP

T/C
THICKNESS TO CHORD RATIO

TAPER
WING TAPER RATIO

The following is a sample input file that computes the zero-lift drag (ID1=5):

```
IOPTIM = 0
IPRINT = 0
IFUNCK = 1
IFLD   = 0
ISR    = 0
ID1    = 5
IPRT   = 0
IDERIV = 1
IHIST  = 0
IPTDET = 0
IWTEQN = 1
NJ     = 0
MBEGIN = 0.75
MSTEP  = 0.2
--------------
INITIAL POINT
--------------
AR     =     7.0
SW     =  3800.0
H      = 32000.0
Sweep  =    21.3
T/C    =    0.10
Taper  =    0.30
```